Anomalous Diffusion and Mixing due to Islands of Tori in Hamiltonian Dynamical Systems

石崎, 龍二
九州大学理学研究科物理学専攻

https://doi.org/10.11501/3065447

出版情報：九州大学, 1992, 博士（理学）, 課程博士
バージョン：
権利関係：

Anomalous Diffusion and Mixing due to Islands of Tori in Hamiltonian Dynamical Systems

石　崎　龍　二

(1)

Thesis

Anomalous Diffusion and Mixing due to Islands of Tori in Hamiltonian Dynamical Systems

Ryuji ISHIZAKI

Department of Physics, Kyushu University 33, Fukuoka 812

December, 1992

Abstract

Anomalous behaviors of the diffusion and mixing of chaotic orbits due to the intermittent sticking to the islands of normal tori and accelerator-mode tori in a widespread chaotic sea are studied numerically and theoretically for Hamiltonian systems with two degrees of freedom. The probability distribution functions for the coarse-grained velocity (characterizing the diffusion) and the coarse-grained expansion rate (characterizing the mixing) turn out to obey an anomalous scaling law which is quite different from the Gaussian. The scaling law is confirmed for both diffusion and mixing by numerical experiments on the standard map and the heating map. Its scaling exponents for the diffusion and mixing, however, are found to be different from each other, indicating that different islands give different scaling exponents.

Contents

§1. Introduction – reconsider classical mechanics by chaos

One of the purposes of this thesis is to understand the motion of a frictionless pendulum. It may be said that "That needs no explanation at this time". To be sure, the frictionless pendulum continues to oscillate in constant rhythm as regular as clockwork. As soon as a periodic external force acts on the pendulum, however, the motion becomes complex. In a particular case, the motion becomes very complex, and the future of the motion is not able to predict. It is common sense that we can not predict the future, when the many factors are generally involved in it. But in this case, we can not predict the future though rule is clear, and the degrees-of freedom are only two and the external force is not random but regular. This strange phenomenon is called chaos.[1)~3)]

The discovery of chaos has greatly influenced science. Let us first review the representative studies and the meaning of chaos in science.

Look back on the history of science, it was Newton to indicate that we can predict the behavior of matters if we know the rule of the motion. Kepler's laws explained how planets move around the sun. In contrast to this, Newton tried to explain the motive power which causes such a motion. He guessed from the law of inertia and Kepler's law that the planets continue to be pulled by the sun. He found that the intensity of the force is in inverse proportion to the second power of the distance between the sun and the planet. Kepler's law has been completely explained by his theory. He also guessed that the attractive force acts between the earth and the moon, and explained the phenomena of tide. He guessed

further that all matters on the earth are pulled by the earth, and explained the free fall and the motion of pendulum, etc. Newton showed that the motive power of celestial motion and motions of matters around us are the same, and explained the time evolution of motion of matters. Then we have been able to understand the motion of planets, comets, moon and pendulum, etc. This is the so-called law of universal gravitation, where gravitation acts between all matters. He expressed the motion in the differential equation and showed that we can understand the motion if we can solve the equation. By Newtonian mechanics, we can predict how the state of motion changes with time if we know what forces acts on the matter and know the motion state (place and velocity of the matter) at an initial time.

We became to be able to understand behavior of matter by deterministic law. Physicists have simplified complex phenomena to understand them and discovered regularities in them. Irregularities have recently been discovered though they simplified things. Though rule is clear, it is not able to predict the future. That is due to chaos. As a remarkable example, let us take the Lorenz model.

Lorenz constructed a simple model to explain the complex motion of the atmosphere. First, suppose a layer of fluid of infinite horizontal extent, heated from below, as shown in Fig.1(a). When the Rayleigh number $Ra(= d^3 g\gamma\Delta T/\nu a)$ – where ΔT is the temperature difference between the bottom and top plates, d the height between the bottom and top plates, g the acceleration of gravity, γ the coefficient of cubical expansion, ν the kinematic viscosity and a the thermal conductivity – exceeds a critical value, the static state of fluid

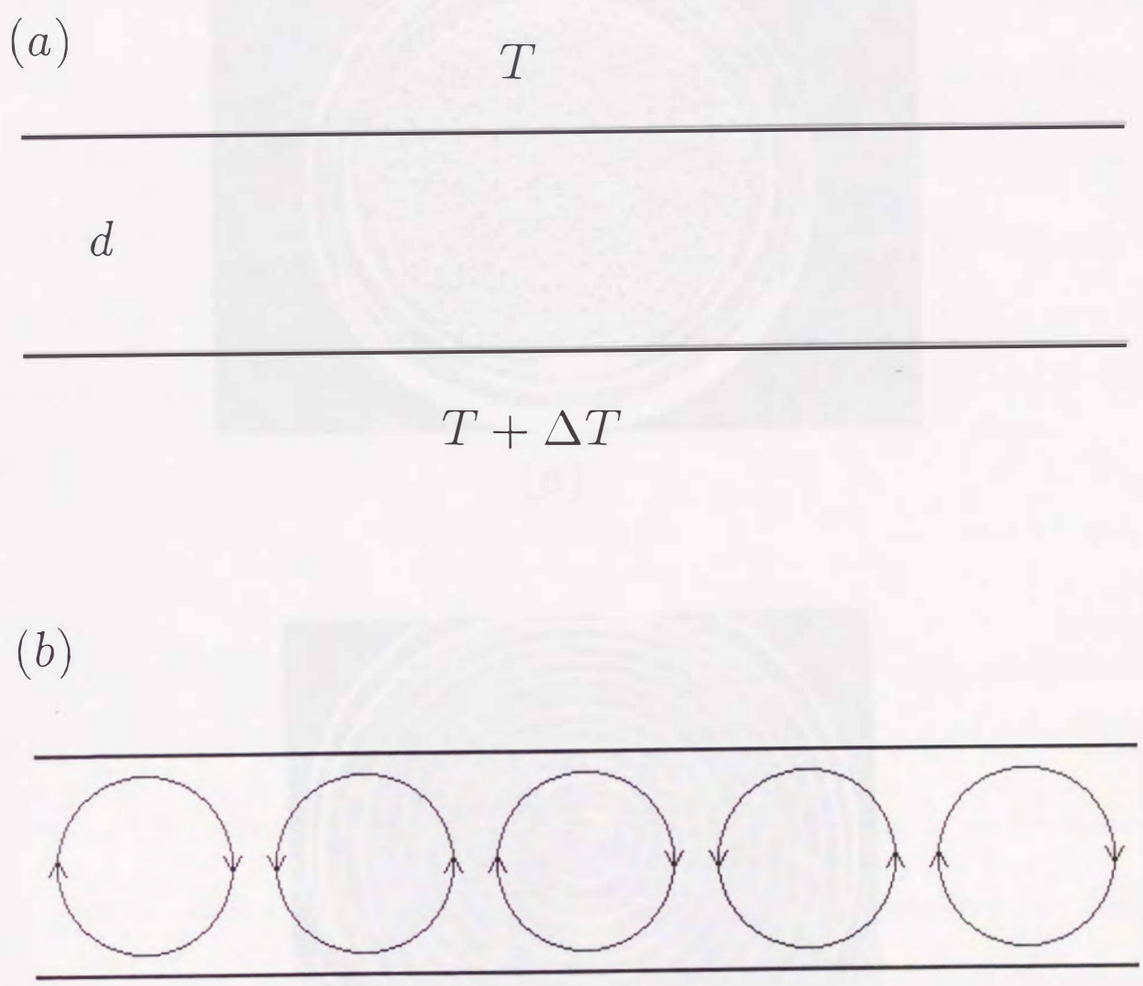

Fig.1 (a) The layer of fluid of infinite horizontal extent with a temperature difference ΔT between the bottom and top plates. (b) Rayleigh-Bénard convection where rising current and descending current are combined.

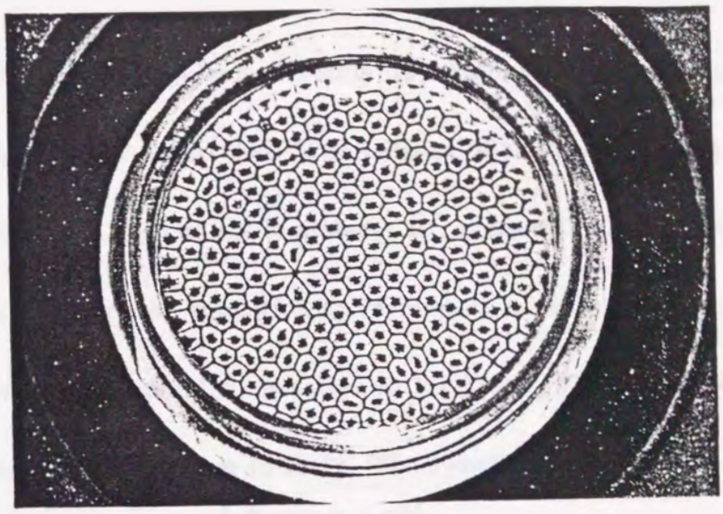

(a)

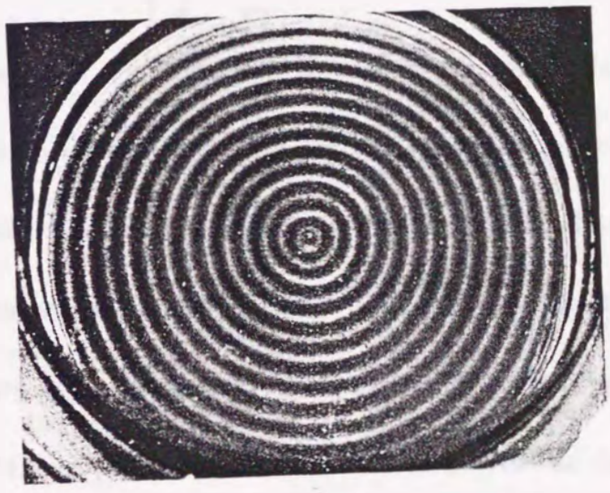

(b)

Fig.2 (a) Hexagonal convection cells on a uniformly heated copper plate in a circular container and open to air surface. Fluid is silicon oil. Visualization with aluminum powder. (E.L. Koschmieder, Adv. chem. Phys. **26**, 177 (1974)) (b) Circular concentric rolls on a uniformly heated copper plate in a circular container and not open to air surface. (E.L. Koschmieder, Adv. chem. Phys. **26**, 177 (1974))

becomes unstable and the regular convection appears, as shown in Fig.1(b). This is the so-called Rayleigh-Bénard convection. The pattern of the convection is various whether the surface of the fluid is open or not to ambient air, as shown in Fig.2. As the temperature difference becomes larger, the transition to turbulence is observed. Lorenz assumed that the convection rolls are all parallel, as shown in Fig.1(b). Then he reduced the number of variables that describe this system to three. The equations are

$$\begin{cases} \dot{X} = -\sigma + \sigma Y, \\ \dot{Y} = -XZ + rX - Y, \\ \dot{Z} = XY - bZ, \end{cases} \tag{1.1}$$

where X is the amplitude of the convection motion, Y the amplitude of the temperature fluctuation, Z a uniform correction to the vertical temperature profile, σ the Prandtl number, r the normalized Rayleigh number and b a parameter related to the horizontal wave vector. These equations are the so-called Lorenz model. He discovered that these equations produce very complex motion. As a matter of surprising fact, the deviation becomes larger with time if the initial value is shifted a little, as shown in Fig.3. This means that the prediction of future is impossible because error of observation is rapidly magnified. This is called "sensitivity to initial conditions." Is this motion completely random, then? The dynamical motion is understood as the trajectories in the phase space. Figure 4 draws the motion in the phase space. The motion whose time series look random produces a very symmetrical form in the phase space. This means that the Lorenz model produces complex motion in the very symmetrical form. He showed further the possibility

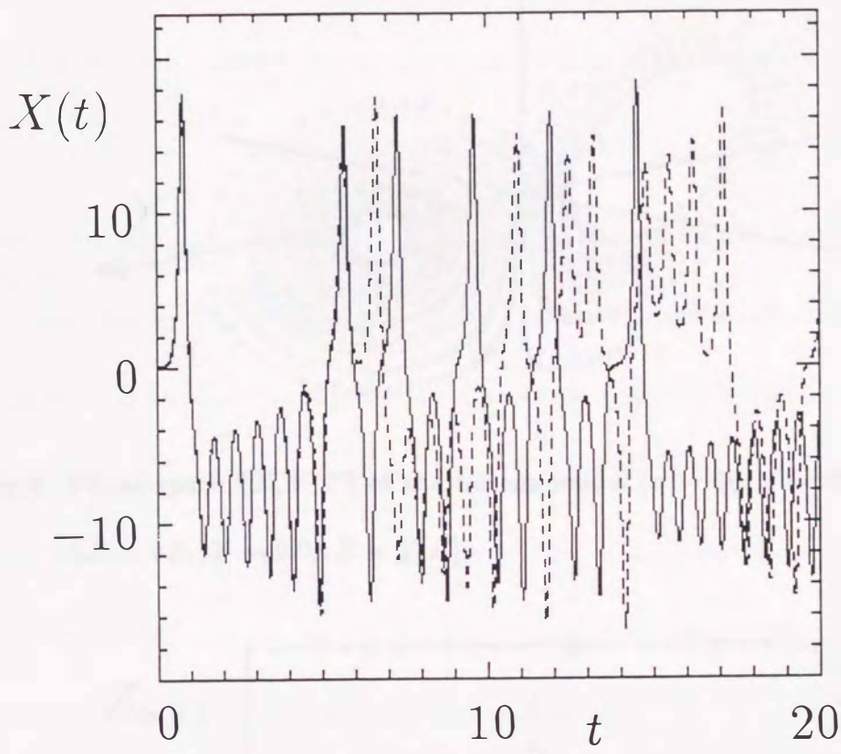

Fig.3 Sensitivity to initial conditions in the Lorenz model ($\sigma = 10$, r = 28, b= 8/3). Evolution of $X(t)$ for two initial condition $\{X_1 = 0.0,\ Y_1 = 0.1,\ Z_1 = 27.0\}$ (full line) and $\{X_2 = 0.0,\ Y_2 = 0.11,\ Z_2 = 27.0\}$ (broken line).

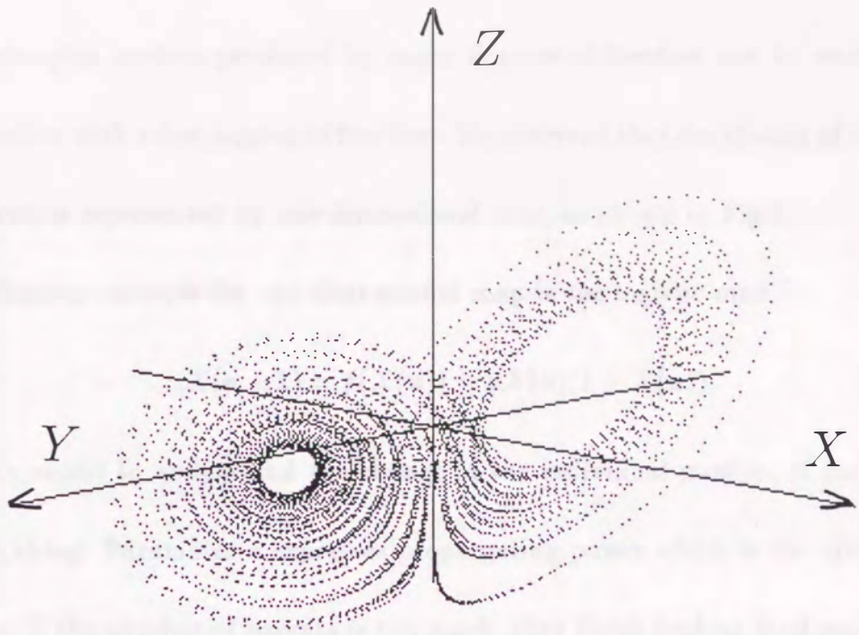

Fig.4 Phase space $\{X, Y, Z\}$ of the Lorenz model (σ = 10, r = 28, b= 8/3). The origin is $\{X = 0.0,\ Y = 0.0,\ Z = 27.0\}$.

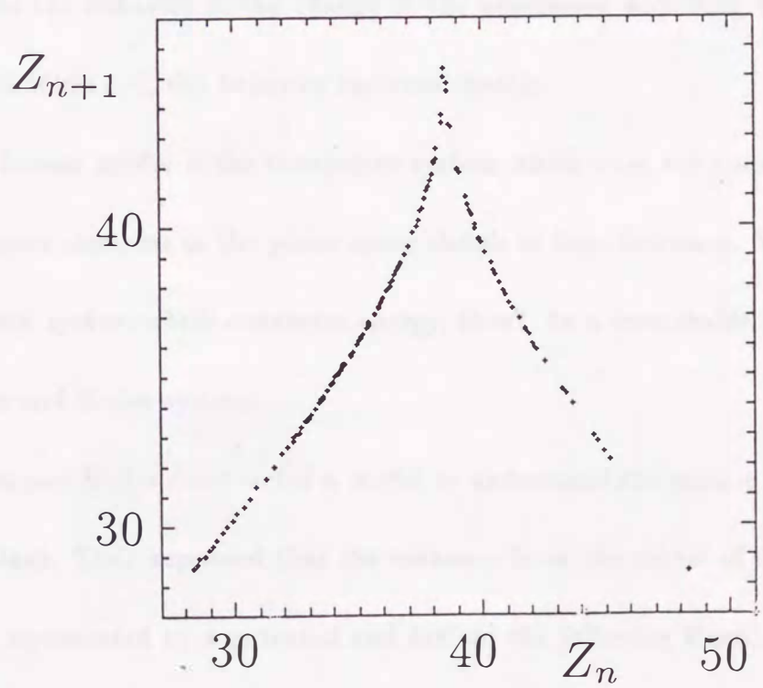

Fig.5 Z_{n+1} vs Z_n, where Z_i are successive maxima of Z for the Lorenz model (σ = 10, r = 28, b= 8/3).

that the complex motion produced by many degrees-of-freedom can be understood as a chaotic motion with a few degrees of freedom. He observed that the change of the maximum in the Z-axis is represented by one dimensional map, as shown in Fig.5.

The famous example for one dimensional map is the logistic map,

$$X(n+1) = f(X(n)) = aX(n)(1 - X(n)). \tag{1.2}$$

This is the model to understand the change of the individual number of each generation of a living thing. Parameter a expresses propergating power which is the ratio of children to parents. If the number of parents is too much, they finish feed on food and the number of children's generation decreases. The $(1 - X(n))$ is in proportion to the amount of food. We can understand how complex motion is produced by this simple rule. Figure 6 expresses the behavior of the change of the generation according to parameter a. For $a > a_c(= 3.56994\cdots)$, the behavior becomes chaotic.

The Lorenz model is the dissipative system which does not conserve energy and for which volume elements in the phase space shrink as time increases. What is chaos in the Hamiltonian system which conserves energy, then? As a remarkable example, let us take the Hénon and Heiles system.

Hénon and Heiles constructed a model to understand the motion of star which moves in the Galaxy. They supposed that the influence from the others of stars to a star in the Galaxy is represented by a potential and derived the following Hamiltonian

$$H = \frac{1}{2}(P_x^2 + P_y^2) + \frac{1}{2}(X^2 + Y^2) + (X^2Y - \frac{1}{3}Y^3), \tag{1.3}$$

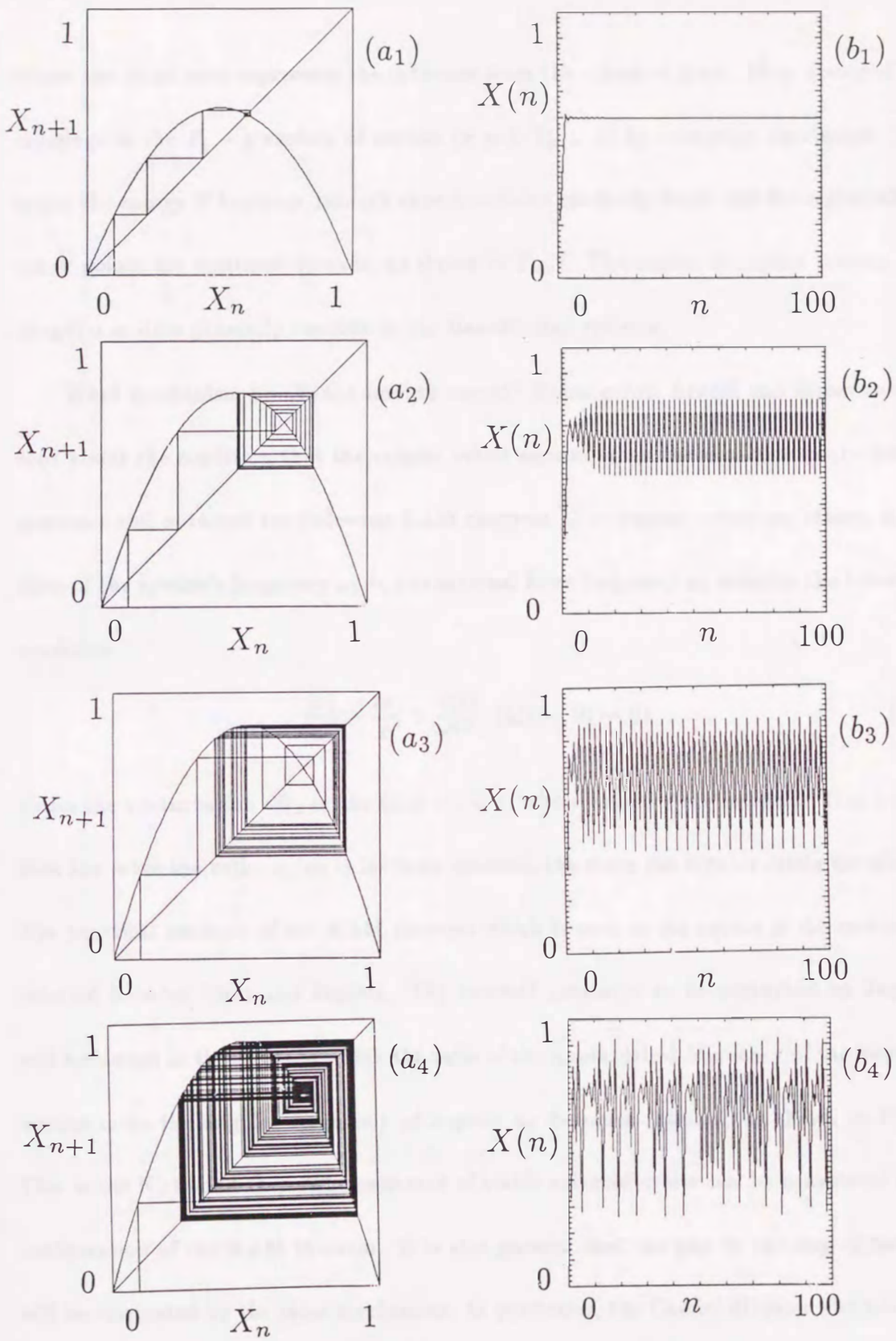

Fig.6 The behavior of the logistic map for $(a_1)(b_1)a = 2.5$: period 1, $(a_2)(b_2)a = 3.2$: period 2, $(a_3)(b_3)a = 3.5$: period 4 and $(a_4)(b_4)a = 3.7$: chaos.

where the third term represents the influence from the others of stars. They observed the crossings in the $P_y - y$ surface of section ($x = 0, P_x > 0$) by computer simulation. The larger the energy E becomes, smooth curved surfaces gradually break and the region where many points are scattered spreads, as shown in Fig.7. The region of regular motion and irregular motion generally coexists in the Hamiltonian systems.

What mechanism breaks the smooth curves? Kolmogorov, Arnold and Moser considered about the condition that the regular orbits survive when the nonlinear perturbation increases and obtained the following KAM theorem. The regular orbits are stable, if the ratio of the system's frequency ω_1 to the external force frequency ω_2 satisfies the following condition

$$|\frac{\omega_1}{\omega_2} - \frac{m}{s}| > \frac{k(\epsilon)}{s^{2.5}} \quad (k(\epsilon \to 0) \to 0) \tag{1.4}$$

under the perturbation ϵH_1 in the limit $\epsilon << 1$, where m and s are integers. This means that the more the ratio ω_1/ω_2 is far from rational, the more the regular orbits are stable. The practical example of the KAM theorem which is seen in the nature is the motion of asteroid between Mars and Jupiter. The asteroid continues to be perturbed by Jupiter and are swept in the orbits in which the ratio of the unperturbed frequency of the asteroid motion ω to the angular frequency of Jupiter ω_j becomes rational, as shown in Fig.8. This is the Kirkwood Gap. The existence of stable asteroid orbits can be considered as a confirmation of the KAM theorem. It is also guessed that the gap in the ring of Saturn will be originated by the same mechanism. In particular, the Cassini division which is the

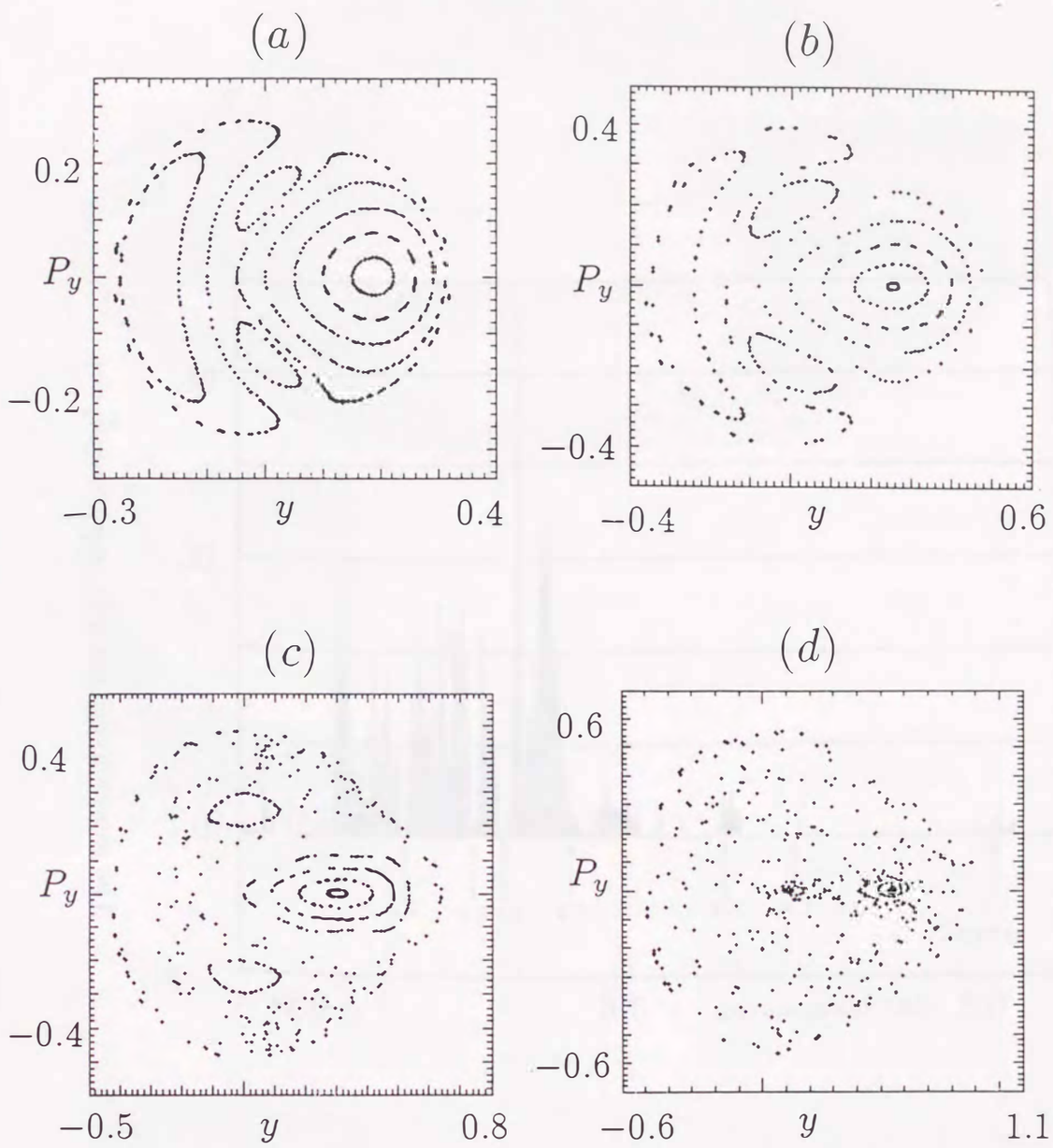

Fig.7 Poincare maps of the Hénon-Heiles system for $(a)E = 1/24$, $(b)E = 1/12$, $(c)E = 1/8$ and $(d)E = 1/6$.

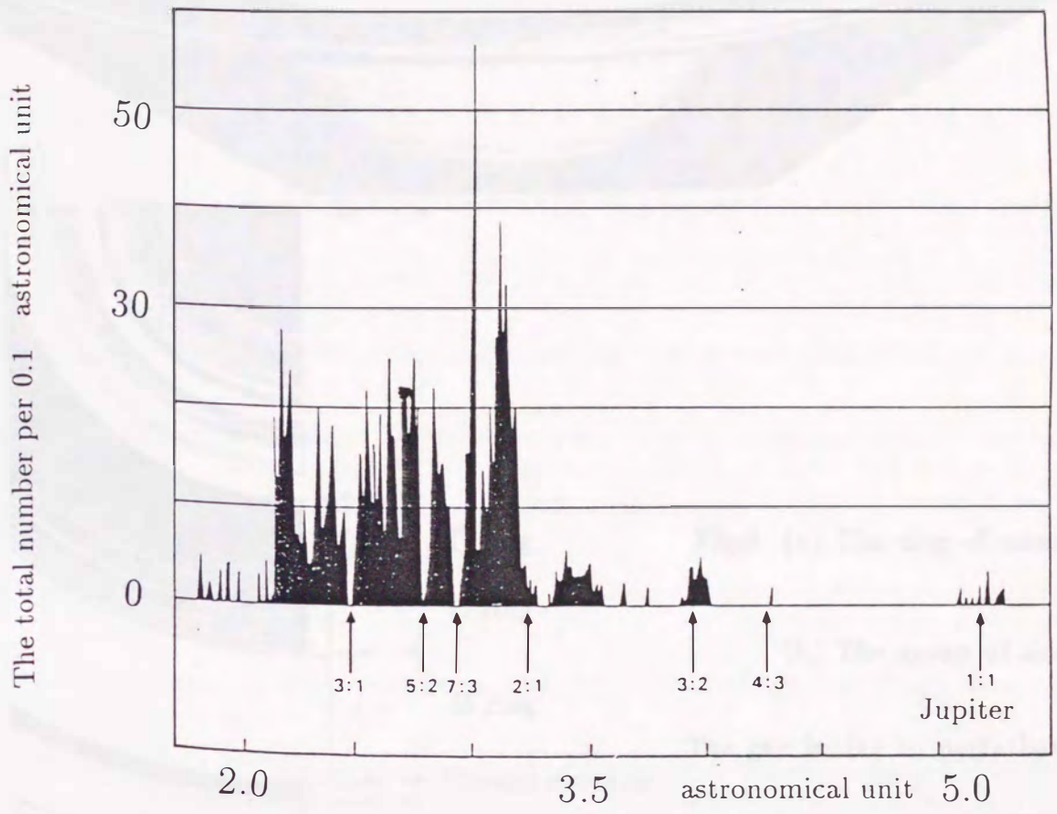

Fig.8 Distribution of asteroids in the belt between Mars and Jupiter. The gap is due to perturbation of Jupiter.

(P.Moore, G.Hunt, I.Nicolson, P.Cattermole, *The Atlas of the Solar System* (Mitchell Beazley Publisher (1981))

(a)

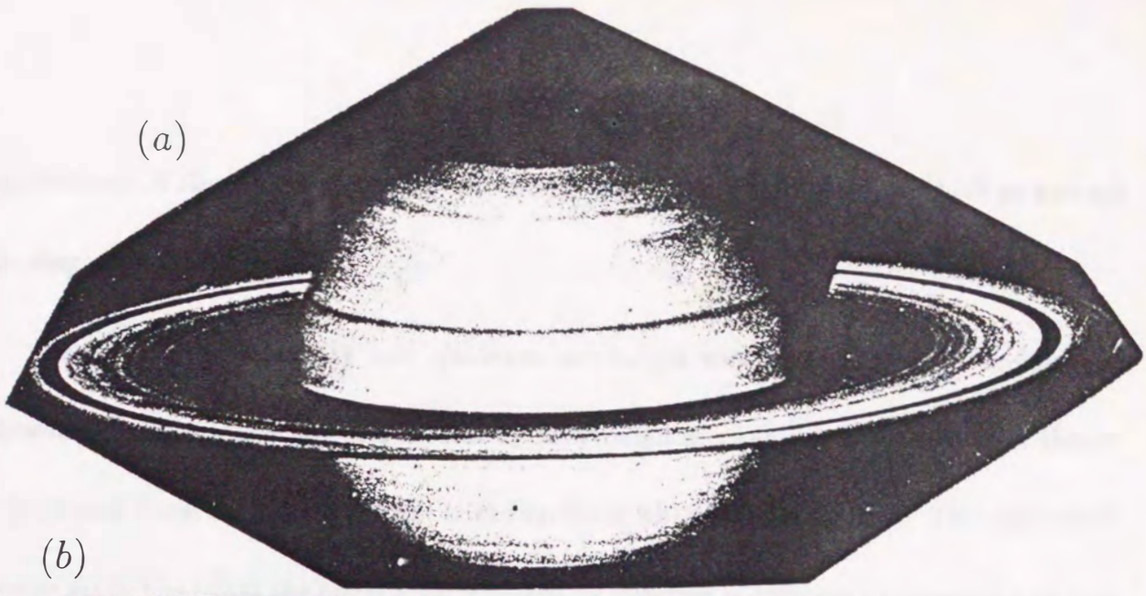

(b)

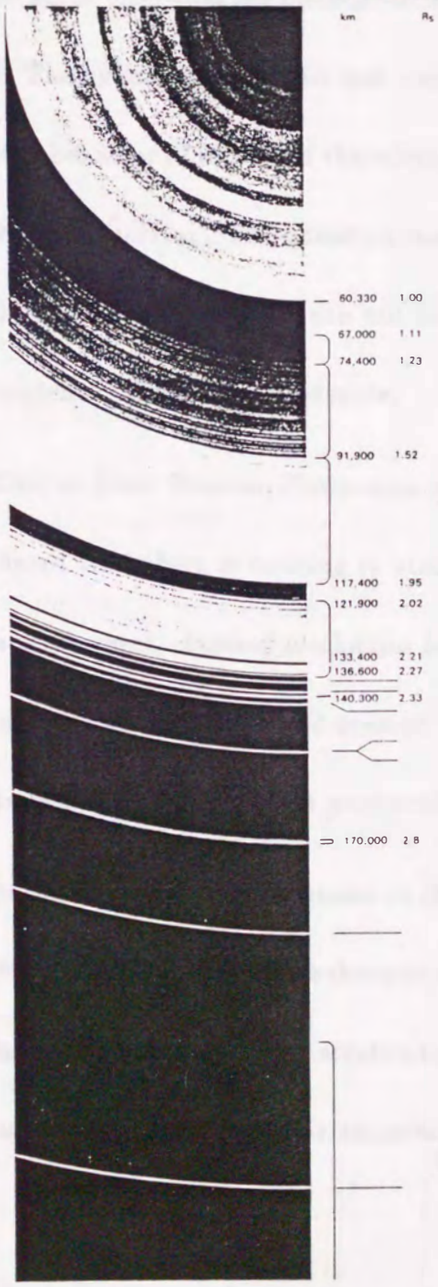

Fig.9 (a) The ring of saturn.

(b) The group of ring.

The gap is due to perturbation of satellite.

(P.Moore, G.Hunt, I.Nicolson, P.Cattermole, *The Atlas of the Solar System* (Mitchell Beazley Publisher (1981))

gap between A ring and B ring is due to the perturbation of the satellites which go around the ring of Saturn.

The theory of relativity and quantum mechanics were constructed to explain the phenomenon which can not understand by Newtonian mechanics. The relativistic theory is produced from the question what is the medium which transmits light. The relativistic theory made clear that the phenomenon looked by observer is different by observer's motion state. The quantum mechanics was constructed from the question how to explain the facts that the behavior of matter in the micro scale looks like either particle or wave according to the way of observing. The quantum mechanics made clear that the place and momentum of particle in the micro scale can not be observed at the same time and we can know only the existence probability of particle.

Due to these theories, Newtonian mechanics is the classical mechanics and physicists considered that there is nothing to study in the Newtonian mechanics. By the discovery of chaos, however, classical mechanics became to be reconsidered. Because it is recognized that the simple systems which seemed very simple produce very complex motion. Then the studies of complex motion produced by simple rule became active.

In this thesis, we shall consider on the behavior of frictionless pendulum. In particular, we shall study the anomalous behaviors of the diffusion and mixing of chaotic orbits caused by islands of normal tori and accelerator-mode tori by taking the standard map and the heating map since they exhibit remarkable statistical properties clearly. In §2, we would

introduce how the behavior of frictionless pendulum is changed by external force. In §3, we consider the deterministic diffusion in the standard map which gives a model for the complex behavior of frictionless pendulum. In §4, we look at the behavior of a small cell in phase space in the heating map. In §5, we introduce the coarse-grained velocity v and its spectrum $\psi(v)$ to study the diffusion of chaotic orbits, and introduce the coarse-grained expansion rate Λ and its spectrum $\psi(\Lambda)$ to study the mixing of chaotic orbits. In §6, we show numerical experiments on these quantities. In §7, we obtain a scaling law for the probability distribution functions of v and Λ by use of Feller's theorem of recurrent events.[18] The last section is devoted to a summary and remarks.

§2. From regular motion to irregular motion of frictionless pendulum

§2.1 The simple pendulum

Let us consider the motion of the simple pendulum, where one edge of the weightless stick of length l is fixed on the point 0 and a mass m is suspended at the other edge of the stick, as shown in Fig.10. The mass m oscillates in the vertical plane. The gravitation mg and tension S from the stick act on this mass. The equation of motion is

$$ml d^2\theta/dt^2 = -mg \sin\theta, \tag{2.1}$$

where θ is the angle between the stick and the vertical line. The integration of this equation by time is

$$(d\theta/dt)^2 = (2g/l)\cos\theta + C, \tag{2.2}$$

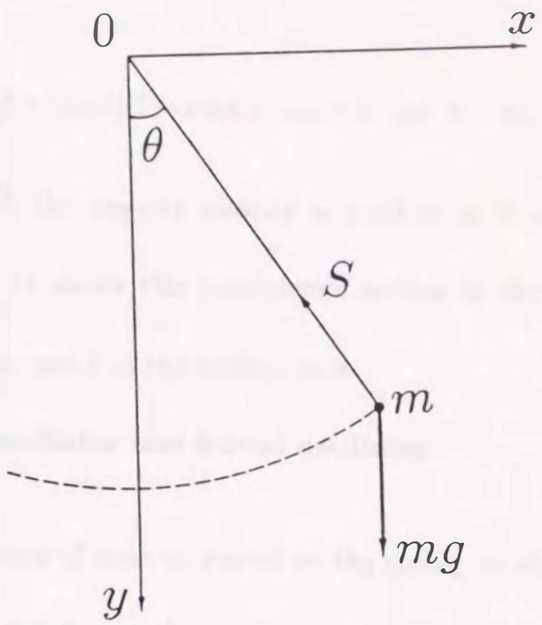

Fig.10 The simple pendulum.

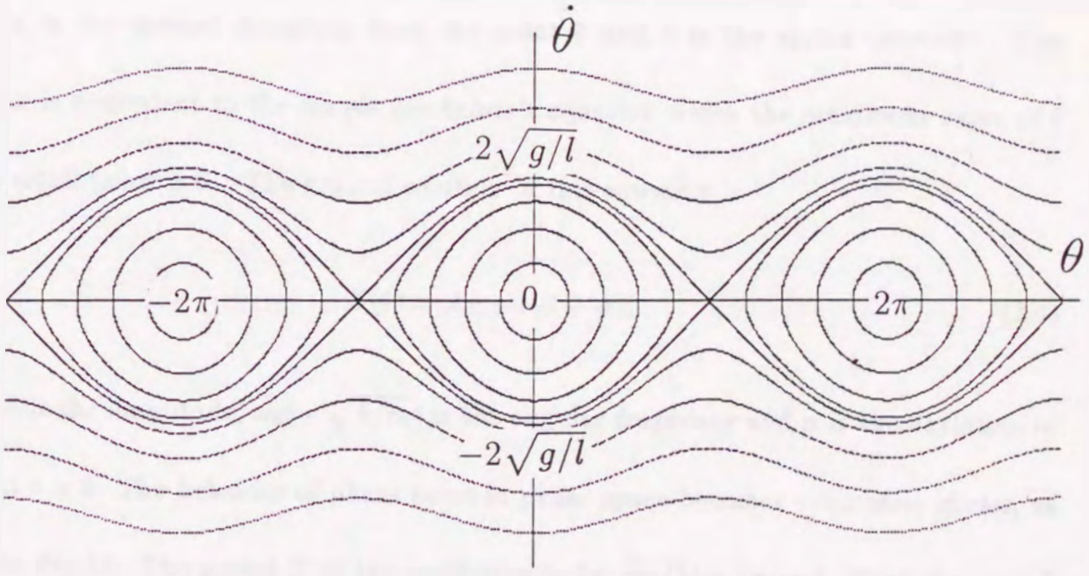

Fig.11 Phase space $\{\theta,\ \dot{\theta}\}$ of the simple pendulum.

$$C = \omega_0^2 - (2g/l)(1 - \cos\theta), \quad \omega_0 = \dot{\theta} \quad (\text{at} \quad \theta = 0).$$

If ω_0 is larger than $2\sqrt{g/l}$, the angular velocity is positive at $\theta = \pi$. Therefore the pendulum rotates. Figure 11 shows this pendulum's motion in the phase space which takes θ in the horizontal axis and $\dot{\theta}$ in the vertical axis.

§2.2. Simple harmonic oscillator and forced oscillator

Let us consider the motion of mass m putted on the spring, as shown in Fig.12. The spring stretches to the point 0 due to the gravitation mg. When the restoring force is proportional to the deviation from the point 0, the equation of the mass m is

$$md^2x/dt^2 = -kx, \tag{2.3}$$

where x is the upward deviation from the point 0 and k is the spring constant. This equation is equivalent to the simple pendulum's equation which the maximum value of θ is very small ($\sin\theta \simeq \theta$). The general solution of this equation is

$$X(t) = A\cos(\omega_0 t + \alpha), \tag{2.4}$$

where A is the amplitude, $\omega_0 (= \sqrt{k/m})$ is the angular frequency and α is the deviation of phase at $t = 0$. The behavior of phase point in phase space becomes concentric circles, as shown in Fig.13. The period T of the oscillation is $2\pi\sqrt{m/k} (= 2\pi/\omega_0)$. Then the period T is independent on the amplitude and depends only on mass m and the spring constant k.

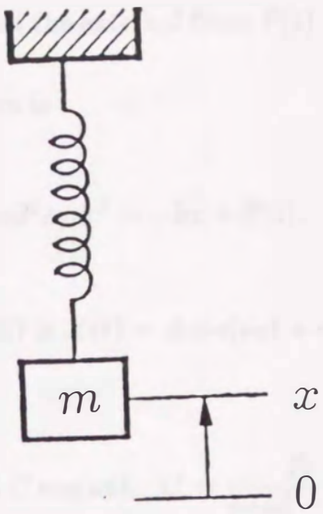

Fig.12 The mass m putted on the spring.

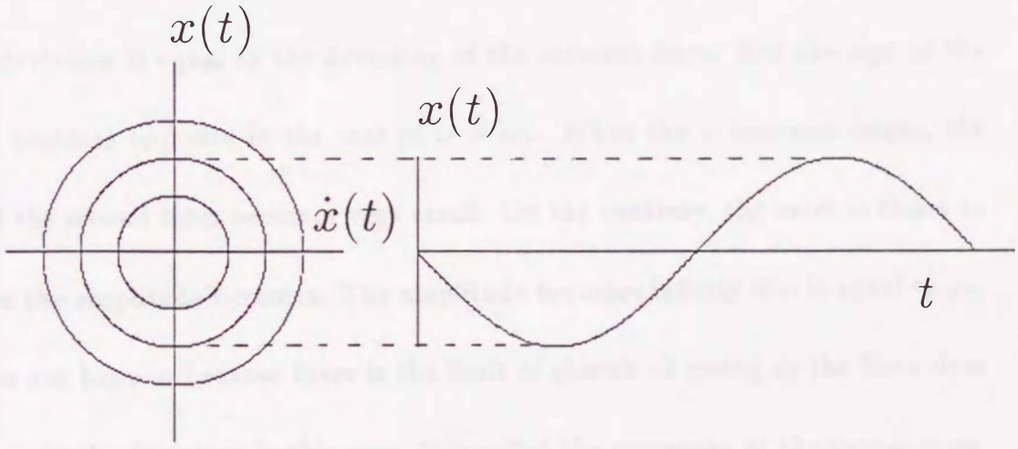

Fig.13 Phase space $\{x,\ \dot{x}\}$ of the simple harmonic oscillator.

In the next, let us consider that the external force $F(t) = F_0 \cos(\omega t)$ acts on the simple Harmonic Oscillator. The equation is

$$md^2x/dt^2 = -kx + F(t). \tag{2.5}$$

The general solution (for $F(t) = 0$) is $X(t) = A\cos(\omega_0 t + \alpha)$. The one particular solution in this case is

$$X(t) = C\cos(\omega t), \quad C = \frac{F_0}{m(\omega_0^2 - \omega^2)}. \tag{2.6}$$

Then the general solution of this equation is

$$X(t) = A\cos(\omega_0 t + \alpha) + \frac{F_0}{m(\omega_0^2 - \omega^2)}\cos(\omega t). \tag{2.7}$$

If the angular frequency ω of the external force is smaller than free frequency ω_0, the direction of deviation is equal to the deviation of the external force. But the sign of the second term becomes opposite in the case of $\omega > \omega_0$. When the ω becomes larger, the amplitude of the second term becomes very small. On the contrary, the more ω closes to ω_0, the larger the amplitude becomes. The amplitude becomes infinity if ω is equal to ω_0. But this does not happen because there is the limit of shirink of spring or the force does not proportion to the deviation in this case. It is called the resonance at the case $\omega = \omega_0$.

§2.3. The periodically kicked rotator

Let us consider the periodically kicked rotator where the periodic external force acts on the frictionless pendulum with no gravitation, as shown in Fig.14. The equation of

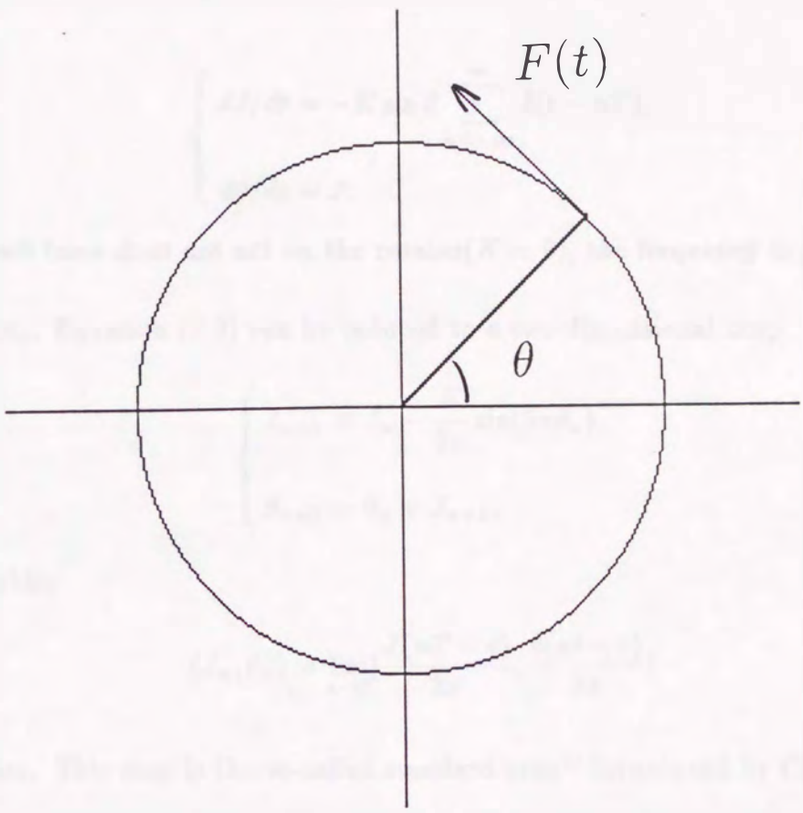

Fig.14 Kicked Rotator.

motion is

$$d^2\theta/dt^2 = -K\sin\theta \sum_{n=-\infty}^{\infty} \delta(t - nT), \tag{2.8}$$

where K is the strength of the external force. The rewritten equations with $J(=\dot{\theta})$ and θ are

$$\begin{cases} dJ/dt = -K\sin\theta \sum_{n=-\infty}^{\infty} \delta(t - nT), \\ d\theta/dt = J. \end{cases} \tag{2.9}$$

If the external force does not act on the rotator($K = 0$), the frequency is proportional to initial velocity. Equation (2.9) can be reduced to a two-dimensional map

$$\begin{cases} J_{n+1} = J_n - \dfrac{K}{2\pi}\sin(2\pi\theta_n), \\ \theta_{n+1} = \theta_n + J_{n+1}, \end{cases} \tag{2.10}$$

for the variables

$$(J_n, \theta_n) = \lim_{\epsilon\to 0}[\frac{J(nT-\epsilon)}{2\pi}, \frac{\theta(nt-\epsilon)}{2\pi}] \tag{2.11}$$

by integration. This map is the so-called standard map[1)] introduced by Chirikov. Figure 15 shows how to change the phase space $\{\theta, J\}$ of the standard map according to parameter K. Figure 16 shows the rime series of J_n for $K = 0.8$. The structure of the phase space is very different from the simple pendulum and the simple harmonic oscillator. The smooth curves represent regular motion (torus) and the region which many points are scattered represents chaotic motion (chaotic sea). Looking figure 15, we can see that regular region (torus) and irregular regions (chaotic sea) are complicated each other. The phase space of a Hamiltonian system generally consists of islands of invariant tori and chaotic seas, and

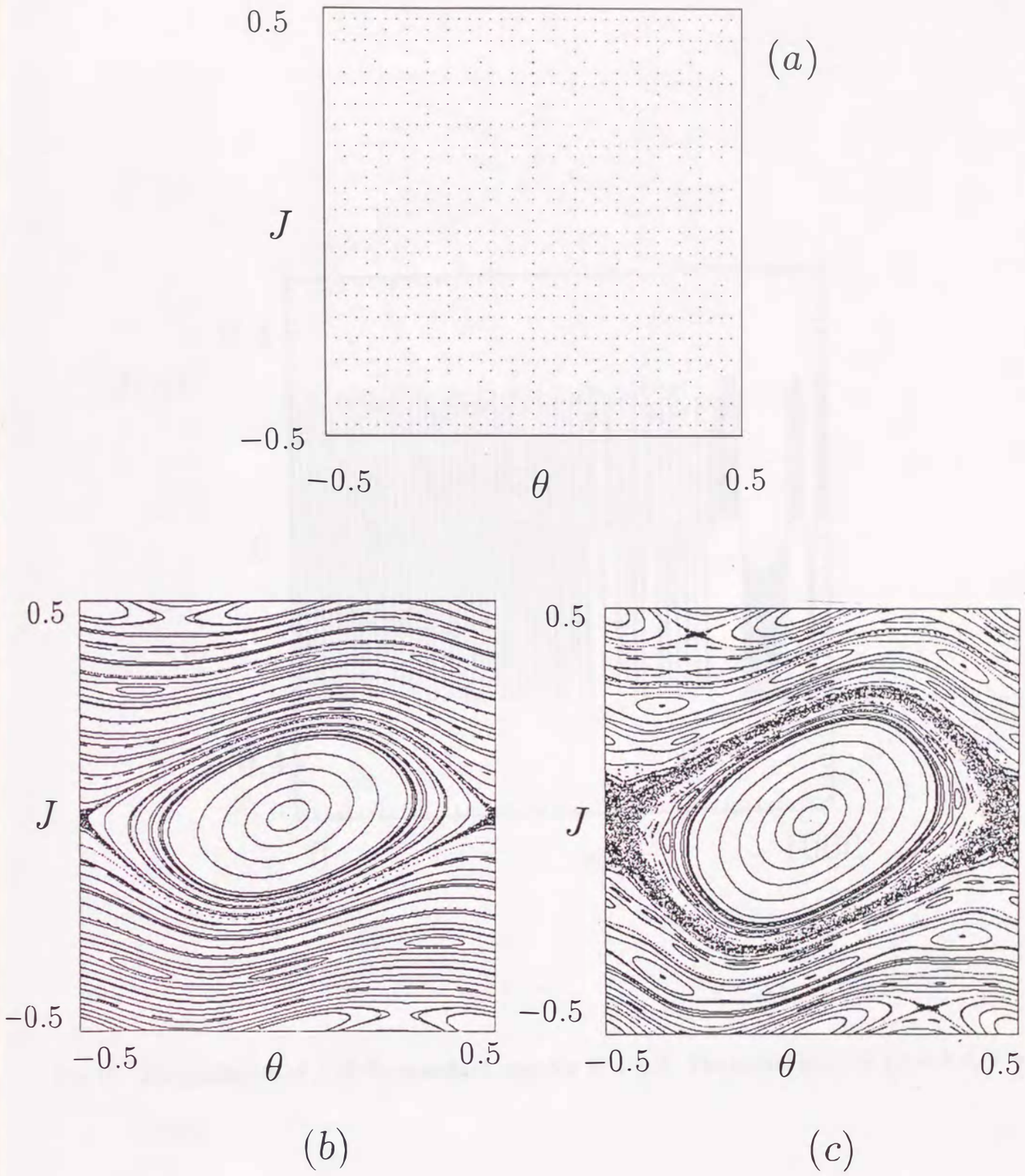

Fig.15 Phase space $\{\theta, J\}$ of the standard map for (a) $K = 0.0$, (b) $K = 0.5$ and (c) $K = 0.8$.

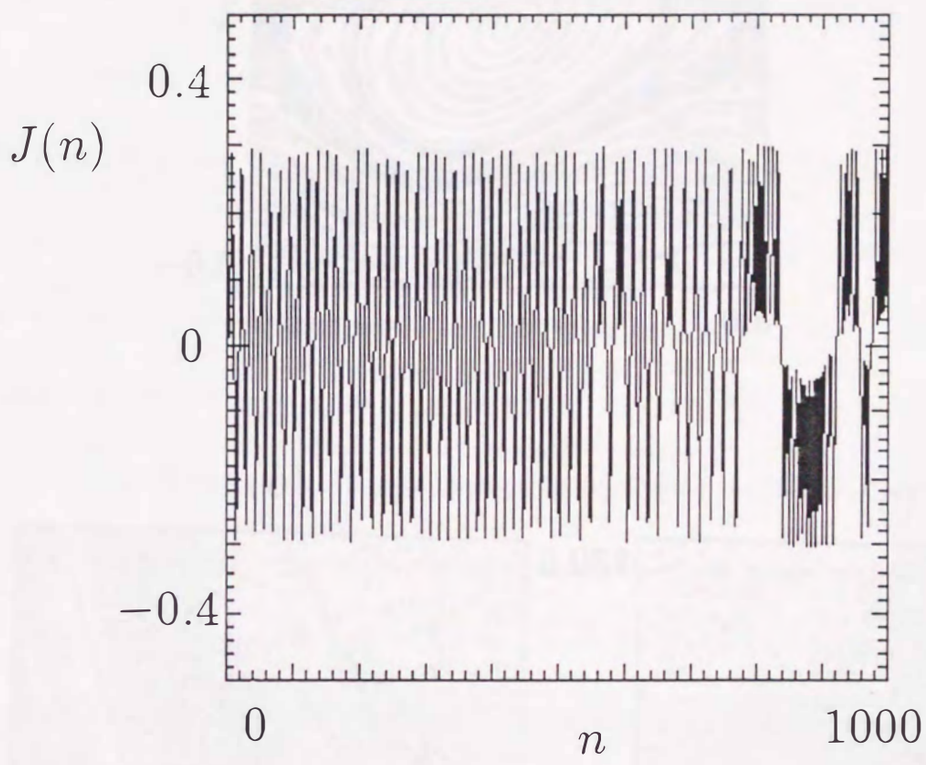

Fig.16 The evolution of J of the standard map for $K = 0.8$. The initial point is $\{J = 0.0,\ \theta = 0.001\}$.

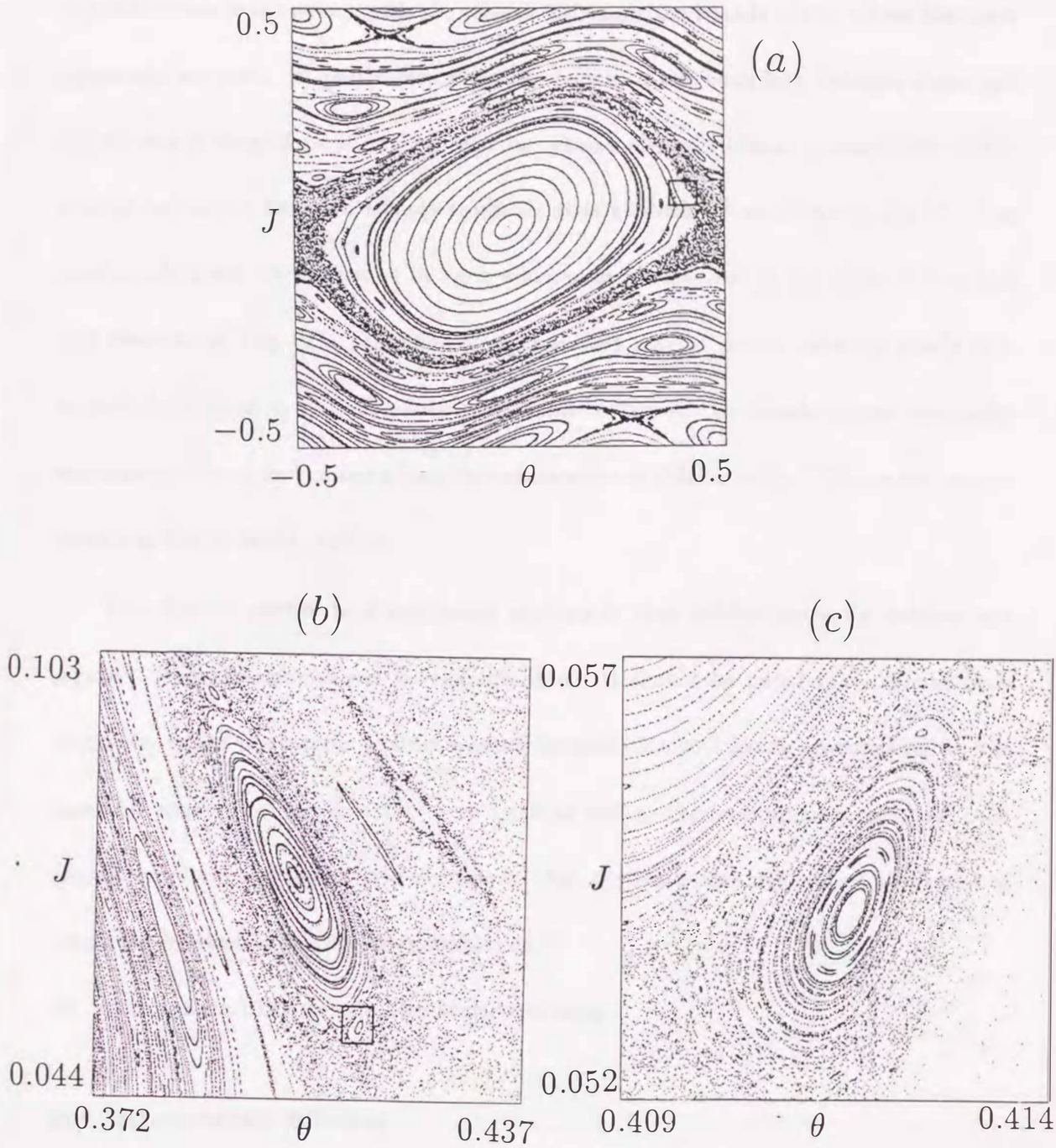

Fig.17 Phase space $\{\theta, J\}$ for (a) $K = 0.8$. (*b*) The magnification of the box of (a). (*c*) The magnification of the box of (b).

any chaotic sea is in contact with the critical tori encircling islands of tori whose Liapunov exponents are zero. In particular, when the region of the boundary between torus and chaotic sea is magnified, it can be seen the chains of small islands around each of the critical tori which have the islands-around-islands hierarchy,[5] as shown in Fig.17. Any chaotic orbits are often trapped by such a hierarchical structure in the chaos border and stay there for a long time, since the local expansion rate of nearby orbits is nearly zero around the critical tori. Such sticking of chaotic orbits to the islands occurs repeatedly and intermittently, and causes a long-time correlation of chaotic orbits.[5] Hence the chaotic motion is not perfectly random.

The chaotic motion in Hamiltonian systems is thus neither perfectly random nor regular. How this motion can be characterized? It should be noted that, though each of chaotic orbits is unstable against a small perturbation and hence unreproducible, the ensemble average of chaotic orbits over a cell as well as the long-time average over each chaotic orbit are stable and reproducible so that the statistical-mechanical properties of chaos can be studied by computer simulation.[4]

§3. Anomalous diffusion in the standard map

§3.1 Deterministic diffusion

For $K > K_c = 0.971635406\cdots$, all the KAM tori which connect $\theta = -0.5$ to $\theta = 0.5$ disappear,[4] as shown in Fig.18(b). In this parameter range ($K > K_c$), there exists a

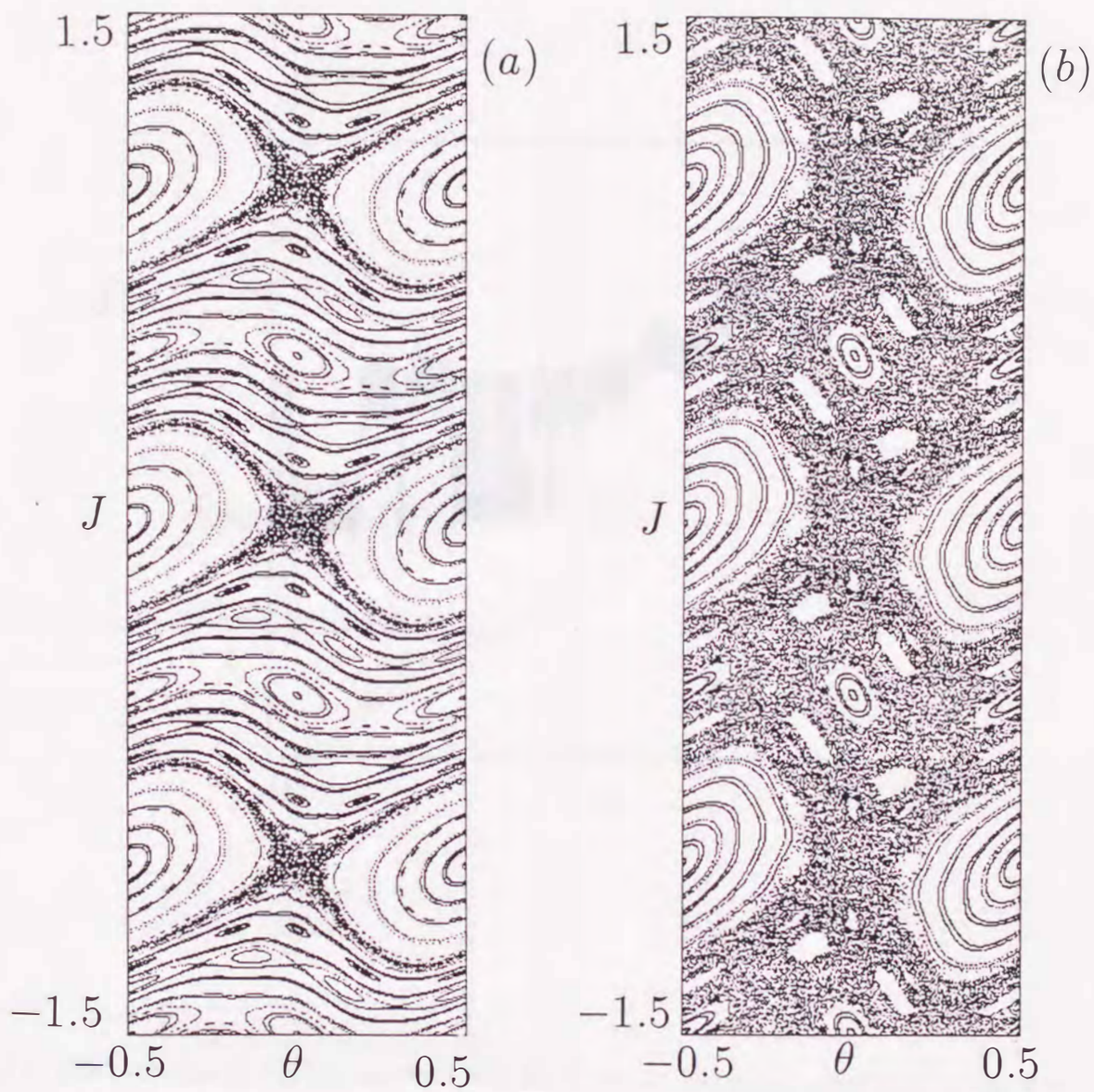

Fig.18 Phase space $\{\theta, J\}$ for (a) $K = 0.8$ where exist the KAM tori which connect $\theta = -0.5$ to $\theta = 0.5$, and (b) $K = 1.2$. All the KAM tori disappear for $K > K_c = 0.971635406\cdots$.

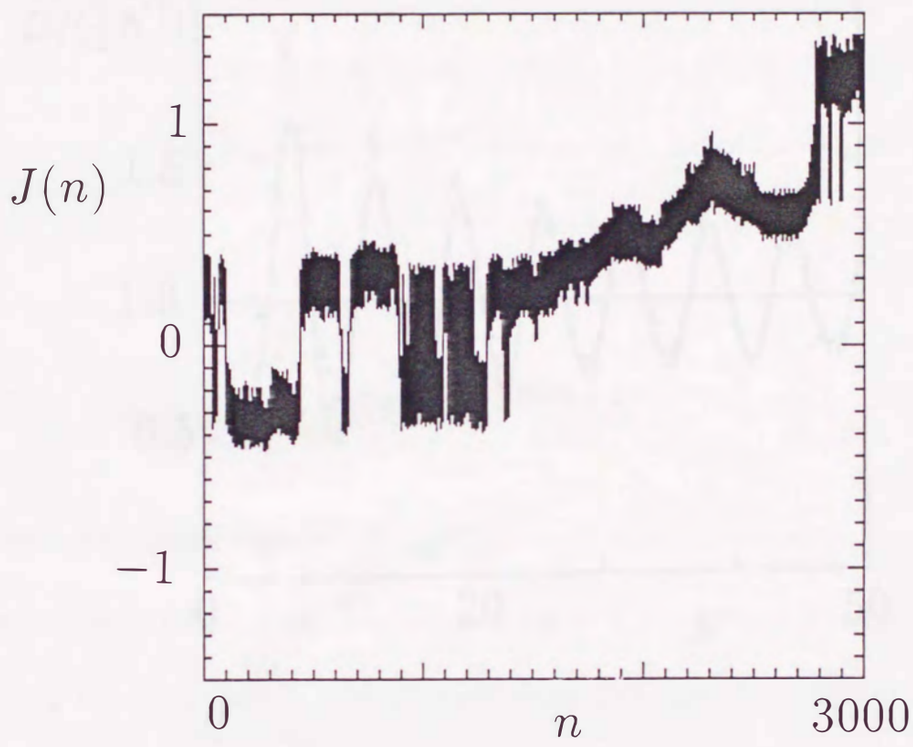

Fig.19 The evolution of J of the standard map for $K = 1.2$. The initial point is $\{J = 0.0,\ \theta = 0.001\}$.

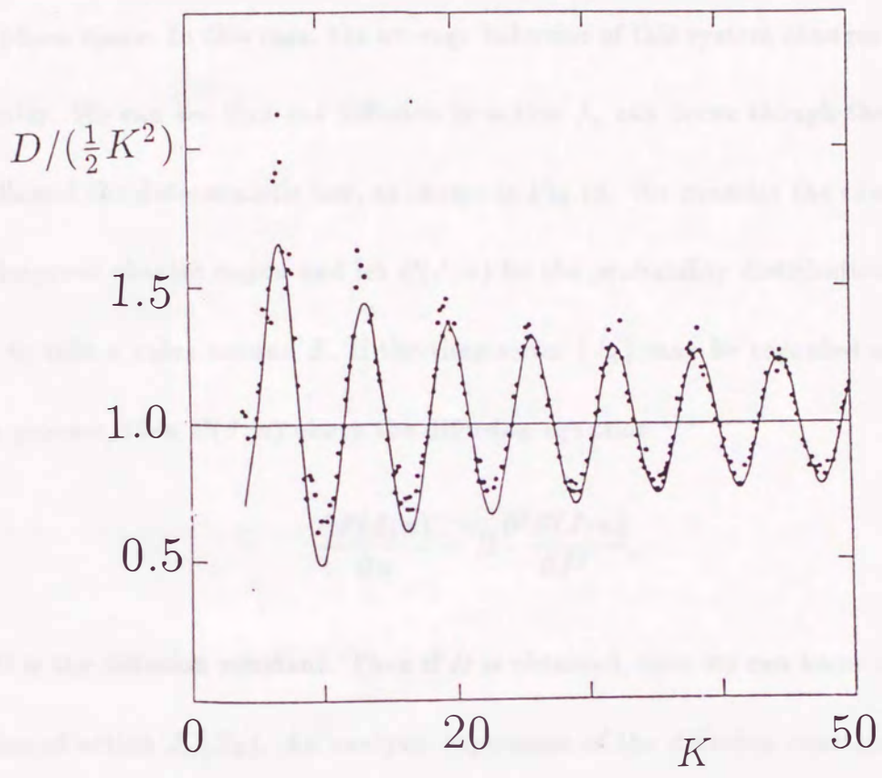

Fig.20 The normalized diffusion constant $D/(\frac{1}{2}K^2)$ vs parameter K in the standard map. The dots are the numerically computed values and the solid line is the theoretical result. (Rechester,A.B. and R.B.White, Phys. Rev. Lett **44** (1980), 1586)

widespread chaotic region which includes the unstable fixed points ($\theta_1^* = 0,\ J_1^* =$ integers). This means that the action J_n can become infinity and the chaotic region occupy most part of phase space. In this case, the average behavior of this system changes from regular to irregular. We can see that the diffusion in action J_n can occur though the evolution of J_n is followed the deterministic law, as shown in Fig.19. We consider the chaotic orbits in this widespread chaotic region and let $P(J;n)$ be the probability distribution function for $J_n(X_0)$ to take a value around J. If the time series $\{J_n\}$ may be regarded as a Gaussian random process, then $P(J;n)$ obeys the diffusion equation [15)]

$$\frac{\partial P(J;n)}{\partial n} = D\frac{\partial^2 P(J;n)}{\partial J^2}, \tag{3.1}$$

where D is the diffusion constant. Then if D is obtained, then we can know the statistical properties of action $J_n(X_0)$. An analytic expression of the diffusion constant D was first obtained by Rechester and White.[15)] Figure 20 shows their analytical result of the diffusion constant and numerical result of the diffusion constant, as the nonlinear parameter K is varied. The analytical result was in good agreement with numerical result of experiments except for the range of parameter K in which the diffusion constant becomes infinity and the diffusion equation (3.1) breaks down. Why does this phenomena happen, then?

§3.2 Anomalous diffusion due to accelerator-mode islands

This is considered due to particular periodic points which are so-called accelerator modes. We consider the periodic points before we explain the accelerator modes.

The linearized matrix of the standard map are

$$M = \begin{bmatrix} 1 & -K\cos 2\pi\theta_n \\ 1 & 1 - K\cos 2\pi\theta_n \end{bmatrix}. \tag{3.2}$$

Eigenvalues of matrix M are

$$\lambda_{\pm} = \frac{2 - K\cos 2\pi\theta_n \pm \sqrt{(2 - K\cos 2\pi\theta_n)^2 - 4}}{2}. \tag{3.3}$$

The stability condition for $\{J_n, \theta_n\}$ yield

$$|2 - K\cos 2\pi\theta_n| \; < \; 2. \tag{3.4}$$

The period 1 fixed points of the standard map are

$$\begin{cases} J_1^* = m, \quad m : \text{integer} \\ \\ \theta_1^* = 0, 0.5. \end{cases} \tag{3.5}$$

The linearized matrix M about fixed points are

$$M = \begin{bmatrix} 1 & \mp K \\ 1 & 1 \mp K \end{bmatrix}. \tag{3.6}$$

The stability condition for fixed points yield

$$|2 \mp K| \; < \; 2. \tag{3.7}$$

Thus the point at $\theta_1 = 0.5$ is always unstable, while for $K < 4$ the elliptic fixed point at $\theta_1 = 0$ is stable. There is no stable motion about period 1 fixed points for $K > 4$.

For a general map, θ is always periodic by 1 but J is not. However, for the standard map, we can consider that J is also periodic by 1. This character causes a second type of

period 1 fixed point. If we consider that the phase and action (both mod 1) are stationary, then we put

$$J_{1l}^{*} = m, \quad \frac{K}{2\pi}\sin 2\pi\theta_{1l}^{*} = l, \qquad m, l : \text{integers.} \tag{3.8}$$

Thus period point is named accelerator modes because the action at the fixed point increases by l for every iteration. The stability condition is replaced by

$$| \, 2 - K\cos 2\pi\theta_{11}| < \; 2$$

and then

$$2\pi|l| < K < \sqrt{(2\pi l)^2 + 16}. \tag{3.9}$$

Islands exist around the periodic point and islands exist around islands in the Hamiltonian systems. The chaotic orbits are trapped by islands when the chaotic orbits approach the islands. When the chaotic orbit enters between islands, it is difficult to go out from this region because of the infinite hierarchical structure of islands. Then the motion is regular for a long time. The action J of chaotic orbit increases by constant interval for this interval. Then the diffusion is enhanced. The structure of islands around the accelerator mode changes as the parameter K is varied, as shown in Fig.21. The accelerator-mode islands are created around a stable periodic orbit $\{X_t^{*}\}$, $(t = 1, 2, \cdots, Q)$ with period Q, which satisfies[16)]

$$J_{t+Q}^{*} - J_t^{*} = l, \quad \frac{K}{2\pi}\sum_{t=1}^{Q}\sin(2\pi\theta_t^{*}) = l, \tag{3.10}$$

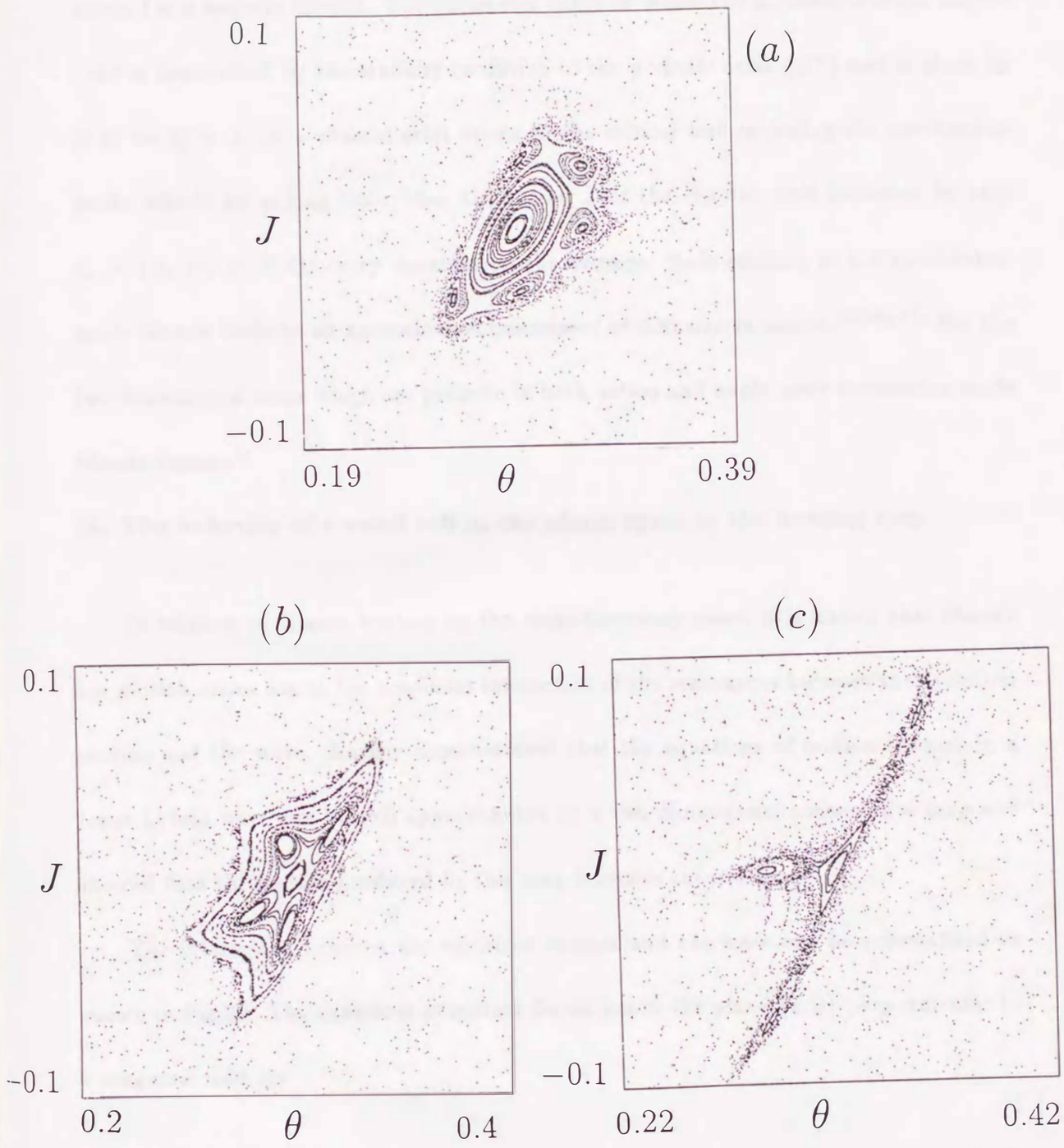

Fig.21 The structures of the islands around the accelerator modes for (*a*) $K = 6.4717$, (*b*) $K = 6.5973$, (*c*) $K = 6.9115$.

where l is a nonzero integer. The parameter range in which the accelerator-mode islands exist is determined by the stability condition of the periodic orbit $\{X_t^*\}$ and is given by (3.9) for $Q = 1$. If a chaotic orbit sticks to the critical tori encircling the accelerator-mode islands for a long time, then the action J of the chaotic orbit increases by step $v_a = \pm v_s, (v_s \equiv |l|/Q)$ every iteration on the average. Such sticking to the accelerator-mode islands leads to an anomalous enhancement of diffusion in action.[10),16),17)] For the two-dimensional maps which are periodic in both action and angle, such accelerator-mode islands appear.[1)]

§4. The behavior of a small cell in the phase space in the heating map

In relation to plasma heating by the radio-frequency wave, it is known that chaotic ion motion arises due to the nonlinear interaction of the resonances between the cyclotron motion and the wave. Karney demonstrated that the equations of motion for ions in a lower hybrid wave can be well approximated by a two-dimensional conservative map and showed that the motion produced by this map becomes chaotic.

The interaction between the cyclotron motion and the wave can be schematized as shown in Fig.22. The equations of motion for an ion in the plane $\{x, y\}$ perpendicular to a magnetic field are

$$\ddot{x} + \Omega^2 x = (qE_0/m)\cos(k_x x - \omega t), \quad \dot{y} = \Omega x, \tag{4.1}$$

where Ω is the cyclotron frequency. If the ion motion does not satisfy the wave-particle

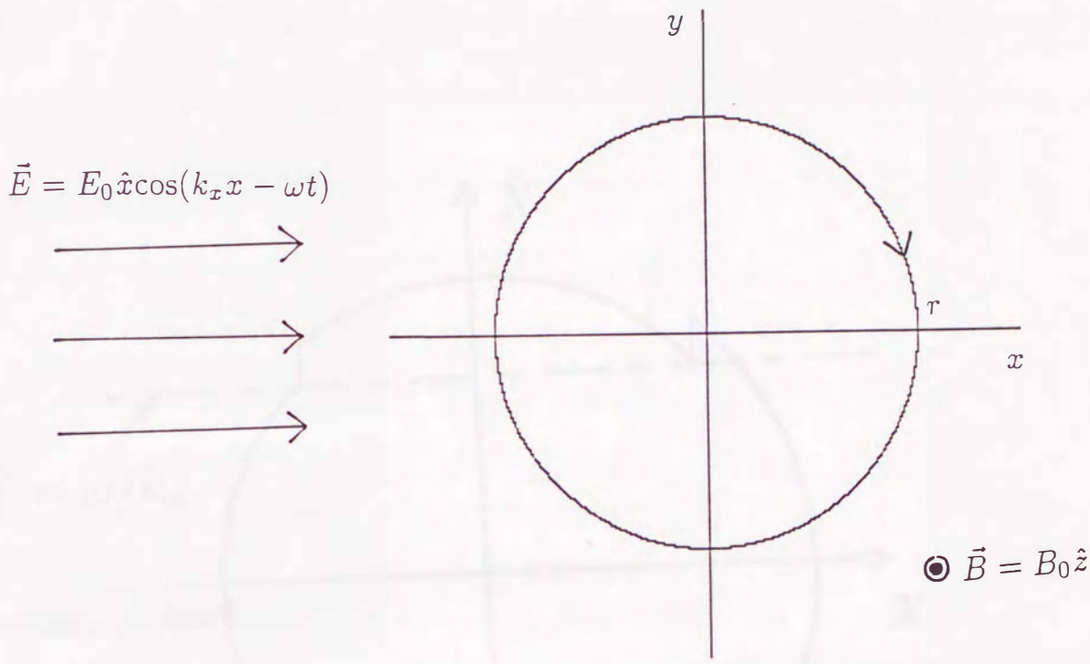

Fig.22 The motion of an ion with mass m and charge q in a coherent lower hybrid wave E with a perpendicular magnetic field B. The cyclotron frequency is $\Omega(= qB_0/m)$ and the Larmor radius is $r(= \sqrt{\dot{x}^2 + \dot{y}^2}/\Omega)$.

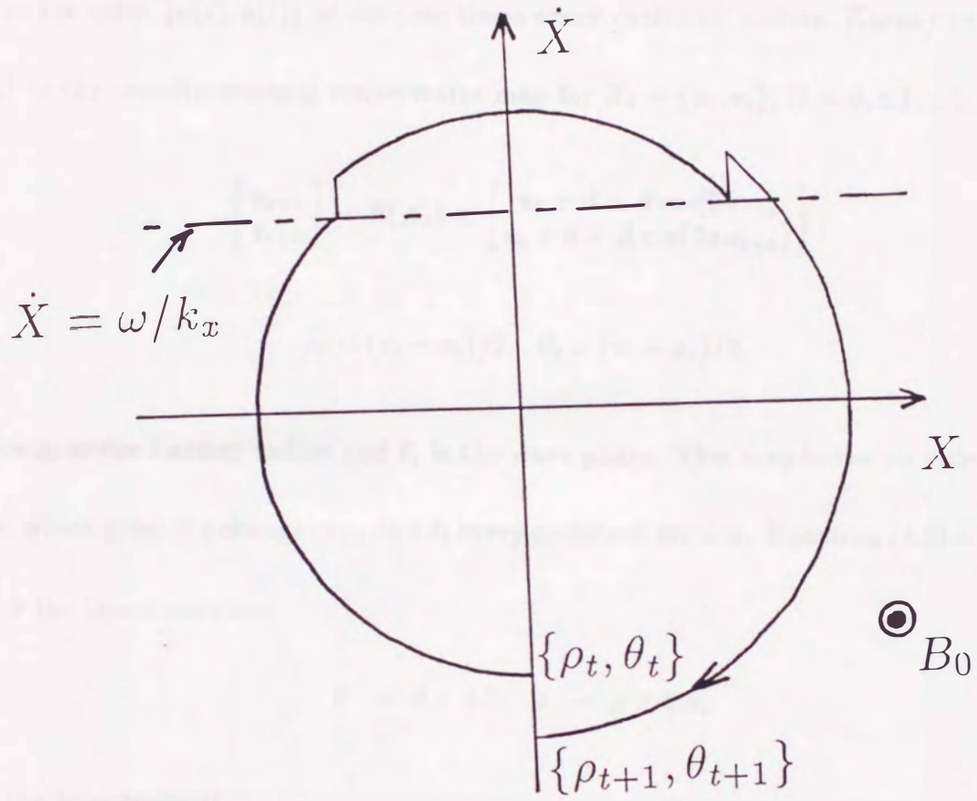

Fig.23 An ion orbit in phase space $\{x, \dot{x}\}$. The ion is kicked at the resonance points on the line $\dot{x} = \omega/k_x$ so that $\{\theta_t, \rho_t\}$ is changed to $\{\theta_{t+1}, \rho_{t+1}\}$ after one cyclotron motion.

resonance condition $\dot{x} = \omega/k_x$, then the ion orbit draws almost a circle with radius $r = (\dot{x}^2 + \dot{y}^2)^{1/2}/\Omega$. But if the Larmor radius r is larger than $\omega/k_x\Omega$, then the resonance points appear twice per one cyclotron motion, as shown in Fig.23. Then, taking the plots of the ion orbit $\{x(t), \dot{x}(t)\}$ at discrete times every cyclotron motion, Karney reduced Eq. (4.1) to the two-dimensional conservative map for $X_t = \{u_t, v_t\}$, $(t = 0, \pm 1, \pm 2, ...)$[13]:

$$\begin{bmatrix} u_{t+1} \\ v_{t+1} \end{bmatrix} = F(X_t) = \begin{bmatrix} u_t + d - A\cos(2\pi v_t) \\ v_t + d + A\cos(2\pi u_{t+1}) \end{bmatrix},$$

$$\rho_t = (v_t - u_t)/2, \quad \theta_t = (v_t + u_t)/2, \tag{4.2}$$

where ρ_t is the Larmor radius and θ_t is the wave phase. This map is the so-called heating map, which gives the change of ρ_t and θ_t every cyclotron motion. Equation (4.2) is invariant under the transformation

$$\theta \rightarrow \theta + 0.5, \quad \rho \rightarrow \rho \pm 0.5, \tag{4.3a}$$

and the time reversal

$$t \rightarrow -t, \quad \theta \rightarrow 0.5 - \theta, \quad \rho \rightarrow \rho. \tag{4.3b}$$

Hence the phase-space structure in $\{\theta, \rho\}$ is symmetric around the vertical line $\theta = 0.25$, as shown in Fig.24. In the following we shall take $d = 0.47$. Then for $A > A_c = 0.20565...$, all the KAM tori which connect $\theta = -0.25$ to $\theta = 0.75$ disappear so that the diffusion in ρ_t can occur,[14] as shown in Fig.24(b). Thus in the parameter range $A > A_c$, there exists a widespread chaotic sea where ρ_t extends over $-\infty < \rho_t < \infty$.

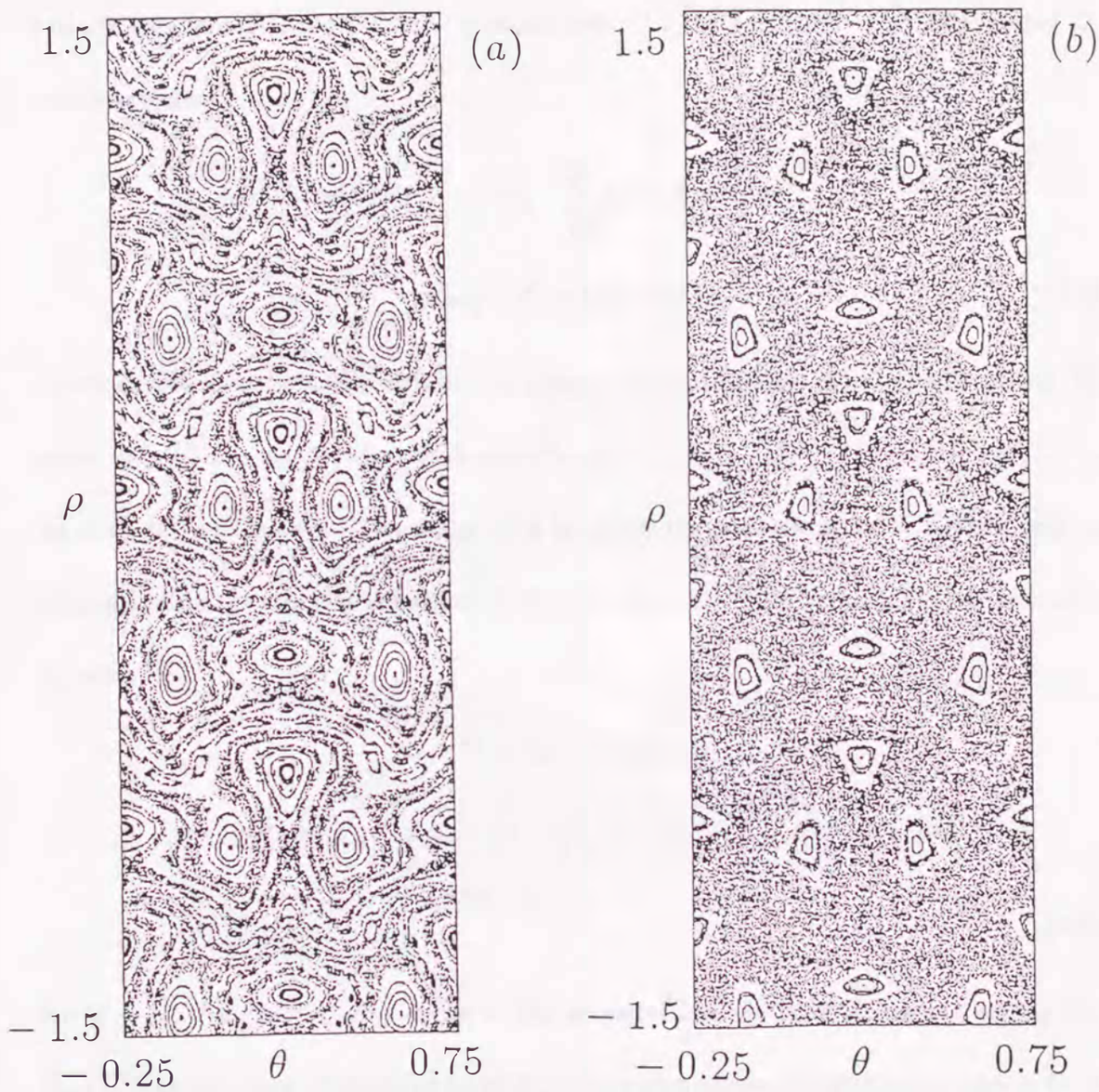

Fig.24 Phase space $\{\theta, \rho\}$ for (a) $A = 0.188$, $d = 0.47$ where exist the KAM tori which connect $\theta = -0.25$ to $\theta = 0.75$, and (b) $A = 0.22$, $d = 0.47$. All the KAM tori disappear for $A > A_c = 0.20565...$ if d is fixed to be $d = 0.47$.

There is also accelerator-modes because ρ is periodic by 0.5. The accelerator-mode islands are created around a stable periodic orbit $\{X_t^*\}$, $(t = 1, 2, \cdots, Q)$ with period Q, which satisfies[17)]

$$\sum_{i=0}^{Q-1}\{d - A\cos(2\pi v_{t+i}^*)\} = -n, \quad \sum_{i=0}^{Q-1}\{d + A\cos(2\pi u_{t+1+i}^*)\} = m,$$

$$\rho_{t+Q}^* - \rho_t^* = (m+n)/2, \tag{4.5}$$

where m and n are integers with $m + n$ being a nonzero integer. The periodic points X_t^* move to $\rho = \pm\infty$ by iteration with definite velocity $v_a \equiv (\rho_{t+Q}^* - \rho_t^*)/Q = \pm v_s, (v_s \equiv |m+n|/2Q)$ in action ρ. The range of A in which the accelerator-mode islands exist is determined by the stability condition of the periodic orbit $\{X_t^*\}$ and is given by $A_l < A < A_u$ with [17)]

$$A_l = \mathrm{Max}(|m-d|, |n+d|),$$

$$A_u = \left[(1/2)\{\ (m-d)^2 + (n+d)^2 + \sqrt{[(m-d)^2 + (n+d)^2]^2 + (4/\pi^4)}\ \}\right]^{1/2} \tag{4.6}$$

for $Q = 1$. If a chaotic orbit sticks to the accelerator-mode islands, staying among the hierarchical structure of chains of small islands around the accelerator-mode islands for a long time, then the action ρ_t of the chaotic orbit increases by step $v_a = \pm v_s$ every iteration.

In order to elucidate how the state point moves in the chaotic sea, let us take a widespread chaotic sea and consider the behavior of a small cell in it that represents numerous state points. Figure 25 shows the time evolution of a thin cell in phase space

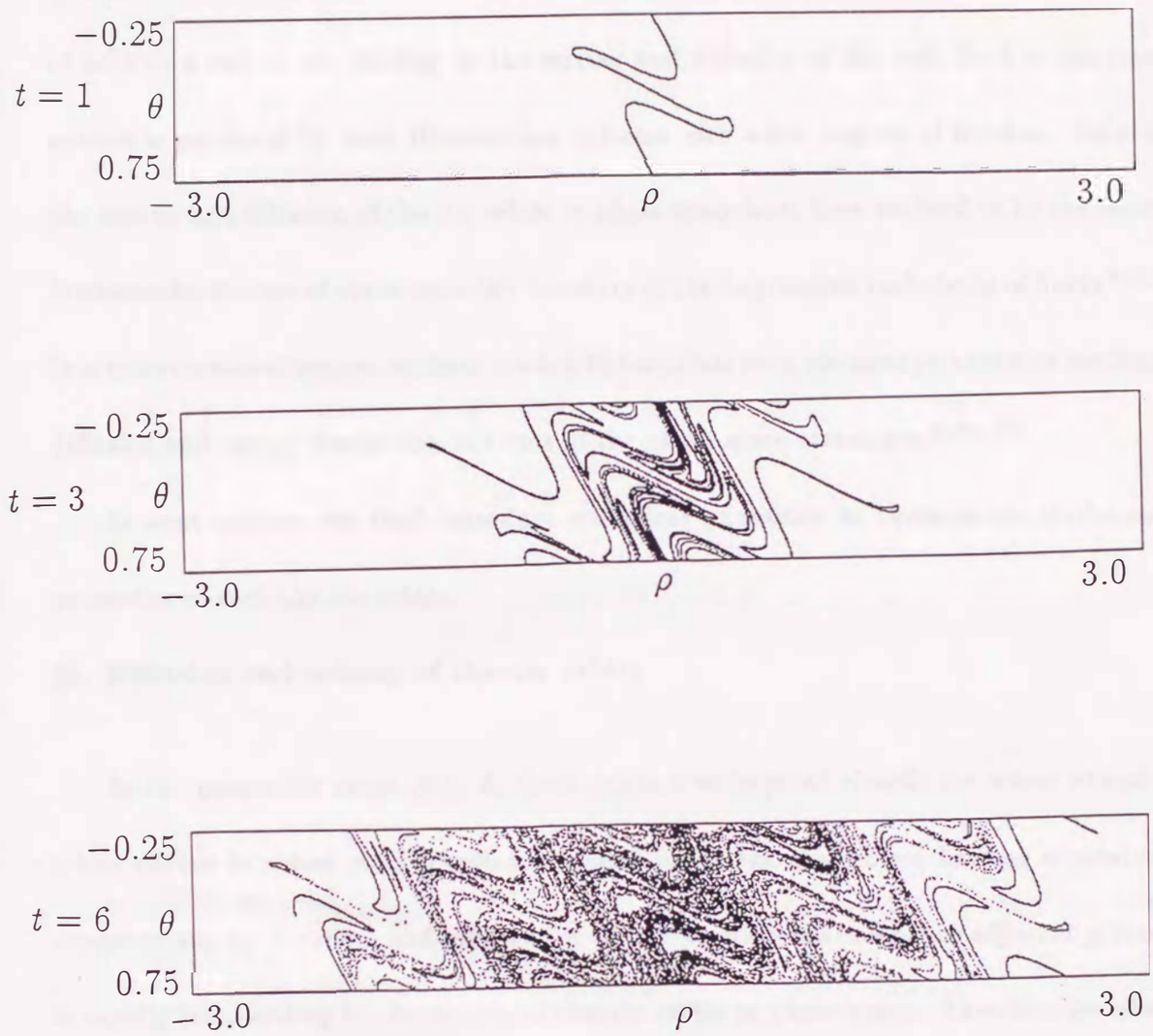

Fig.25 Time evolution of a thin cell in phase space $\{\theta, \rho\}$ of the heating map for $A = 0.50, d = 0.47$. The initial points of the cell at time $t = 0$ whose number is $N = 30000$ lie on the line $\{-0.25 \leq \theta_0 < 0.75, \rho_0 = 0.0\}$ uniformly. Though the cell is stretched and folded with increasing time, its measure is preserved.

$\{\theta, \rho\}$ of the heating map. The cell is stretched and folded with increasing time like a drop of milk in a cup of tea, leading to the mixing and diffusion of the cell. Such a complex motion is produced by most Hamiltonian systems with a few degrees of freedom. Indeed the mixing and diffusion of chaotic orbits in phase space have been realized to be the most fundamental feature of chaos since the discovery of the Lagrangian turbulence of fluids.[6),7)] In a recent series of papers, we have started to formulate such physical processes as mixing, diffusion and energy dissipation in terms of the phase-space structures.[4),8)~12)]

In next section, we shall introduce statistical quantities to characterize statistical properties of such chaotic orbits.

§5. Diffusion and mixing of chaotic orbits

In the parameter range $A > A_c$ there exists a widespread chaotic sea where chaotic orbits diffuse in action ρ. The adjacent points inside the chaotic sea become separated exponentially by iteration, and information on the position relation of the adjacent points is rapidly lost, leading to the mixing of chaotic orbits in phase space. Therefore we now discuss the statistical properties of the diffusion and mixing of chaotic orbits.

§5.1 Diffusion and velocity spectrum $\psi(v)$

We want to know how a thin cell in phase space diffuses with time t. Let us consider the diffusion of a cloud of numerous phase points X_t's, whose number is denoted by N. For numerical experiments we take $N = 10^5$ phase points X_t's which initially lie on the line $\{-0.25 \leq \theta_0 < 0.75, \rho_0 = 0.0 \text{ or } 0.1\}$ uniformly. If the decay of the time correlation of

ρ_t is sufficiently rapid, then the diffusion constant D would exist, leading to the variance

$$< (\rho_n - \rho_0)^2 > = 2Dn \tag{5.1}$$

for $n \gg 1$, where $< \cdots >$ denotes the ensemble average over the N initial points X_0's of the cloud, and $n \ll N$ must be satisfied.

We consider the time series of $u_t \equiv \rho_{t+1} - \rho_t$ which represents the displacement of ρ_t by one iteration. As mentioned in §3,4, the chaotic orbits stick to the accelerator-mode islands repeatedly. Since the value of u_t in the chaos border is far from its average $< u_t >= 0$, we first study the fluctuations of u_t about its average by introducing the coarse-grained velocity[4)]

$$v_n(X_0) \equiv (\rho_n - \rho_0)/n = (1/n) \sum_{t=0}^{n-1} u_t. \tag{5.2}$$

Its probability density is given by $P(v;n) \equiv< \delta(v_n(X_0) - v) >$, where $\delta(g)$ is the δ -function of g. As $n \to \infty$, v_n converges to the average $v_\infty(X_0) =< u_t >= 0$ and $P(v;n)$ decays as $n \to \infty$. We want to know how $P(v;n)$ decays with time n. We may first assume that the decay is exponential for large n so that there exists the velocity spectrum[4)]

$$\psi(v) \equiv \lim_{n\to\infty} \psi_n(v) \quad \text{with} \quad \psi_n(v) \equiv -(1/n) \log[P(v;n)/P(\bar{v};n)], \tag{5.3}$$

where $\bar{v} \equiv< v_n(X_0) >=< u_t >= 0$ and $\psi(v)$ is a concave even function of v with $\psi(v) \geq \psi(0) = 0$. If u_t is Markov, then $P(v;n)$ is Gaussian with $\psi(v) = v^2/4D$.

Equation (5.2) leads to the variance

$$< (\rho_n - \rho_0)^2 > = nC_0 + 2\sum_{t=1}^{n-1}(n-t)C_t, \tag{5.4}$$

where $C_t \equiv < u_t u_0 >$ is the time-correlation function of u_t. In general, we have

$$< (\rho_n - \rho_0)^2 > \propto n^{\zeta}, \quad (0 \leq \zeta < 2) \tag{5.5}$$

for large n. If C_t has a long-time correlation of the form $C_t \propto t^{-(\beta-1)}$ with $1 < \beta < 2$, then the second term of (5.4) leads to $\zeta = 3 - \beta > 1$, so that (5.1) and (3.1) break down with $D = \infty$, leading to $\psi(v) = 0$. This will be called the anomalous diffusion. Indeed such a remarkable situation occurs when an accelerator-mode island exists, as will be shown in section §3, 4.

§5.2 Mixing and expansion-rate spectrum $\psi(\Lambda)$

We want to know how a small cell in the chaotic sea is mixed with time t. The mixing is indispensable for the diffusion. Let us consider a small cell at X_t in the chaotic sea. The small cell is expanded in the local direction along the local unstable manifold and contracted along the local stable manifold, where the area of the cell is preserved for Hamiltonian systems. This process leads to the stretching and folding of the cell, as shown in Fig.25, causing the mixing of chaotic orbits. Therefore the mixing of chaotic orbits is characterized by the local expansion rate $\lambda_1(X_t)$ of a small cell along the local unstable manifold.

The local expansion rate of nearby chaotic orbits at X_t is given by[4)]

$$\lambda_1(X_t) \equiv \log |DF(X_t)u_1(X_t)|, \tag{5.6}$$

where $u_1(X_t)$ is the unit vector tangent to the local unstable manifold at X_t and $DF(X_t)$ is the Jacobian matrix of the map F at X_t. The Liapunov exponent of the orbit $\{X_t\}$ is given by its long-time average

$$\Lambda_\infty(X_0) \equiv \lim_{n\to\infty} (1/n) \sum_{t=0}^{n-1} \lambda_1(X_t). \tag{5.7}$$

We assume that the chaotic sea is ergodic. Then the Liapunov exponent $\Lambda_\infty(X_0)$ is independent of the initial point X_0 for almost all X_0 within the chaotic sea and is simply denoted by Λ^∞, where $\Lambda^\infty = < \lambda_1(X_0) >$ is positive. Nearby chaotic orbits around the islands in the chaos border are not easily separated from each other so that $\lambda_1(X_t)$ is nearly zero there and this situation lasts for a long time. This gives a remarkable effect to the statistical properties of $\lambda_1(X_t)$. Then it is convenient to introduce the coarse-grained expansion rate [4)]

$$\Lambda_n(X_0) \equiv (1/n) \sum_{t=0}^{n-1} \lambda_1(X_t) \tag{5.8}$$

to know how $\lambda_1(X_t)$ fluctuates about the Liapunov exponent Λ^∞. The probability density for $\Lambda_n(X_0)$ to take a value around Λ is given by $P(\Lambda; n) \equiv < \delta(\Lambda_n(X_0) - \Lambda) >$, where $\delta(g)$ denotes the δ-function of g and $< \cdots >$ denotes the long-time average

$$< G(X_0) > \equiv \lim_{N\to\infty} (1/N) \sum_{t=0}^{N-1} G(X_t). \tag{5.9}$$

Similarly to the velocity spectrum (5.3), we introduce the expansion-rate spectrum[4)]

$$\psi(\Lambda) \equiv \lim_{n\to\infty} \psi_n(\Lambda) \quad \text{with} \quad \psi_n(\Lambda) \equiv -(1/n)\log[P(\Lambda;n)/P(\Lambda^\infty;n)]. \tag{5.10}$$

The variance of the sum $S_n(X_0) \equiv n\Lambda_n(X_0)$ with $< S_n >= n\Lambda^\infty$ is given by

$$< (S_n - < S_n >)^2 > = nC_0^\lambda + 2\sum_{t=1}^{n-1}(n-t)C_t^\lambda, \tag{5.11}$$

where $C_t^\lambda \equiv < \hat{\lambda}_1(X_t)\hat{\lambda}_1(X_0) >$ is the time-correlation function of $\hat{\lambda}_1(X_t) \equiv \lambda_1(X_t) - \Lambda^\infty$. In general, we have

$$< (S_n - < S_n >)^2 > \propto n^{\acute{\zeta}}, \quad (0 \le \acute{\zeta} < 2) \tag{5.12}$$

for large n. If C_t^λ has a long-time correlation of the form $C_t^\lambda \propto t^{-(\acute{\beta}-1)}$ with $1 < \acute{\beta} < 2$, then the second term of (5.11) leads to $\acute{\zeta} = 3 - \acute{\beta} > 1$, further resulting in $\psi(\Lambda) = 0$ for $0 < \Lambda < \Lambda^\infty$. This will be called the anomalous mixing. Indeed such a remarkable situation occurs when a visible island exists, as will be shown in §6.2.

The expansion-rate spectrum (5.10) and the variance (5.11) characterize the mixing of chaotic orbits from the statistical-mechanical viewpoint.

§6. Numerical results

In this section we shall show numerical experiments. Parameter values used in computations are (a) $A = 0.50, d = 0.47$ and (b) $A = 0.574, d = 0.47$. Figure 26 shows the phase-space structure for (a) $A = 0.50$ with visible islands where no accelerator-mode islands coexist, and (b) $A = 0.574$ with visible islands where the accelerator-mode islands with $Q = 3, v_s = 1/2$ coexist, as shown in Fig.26(b_3).

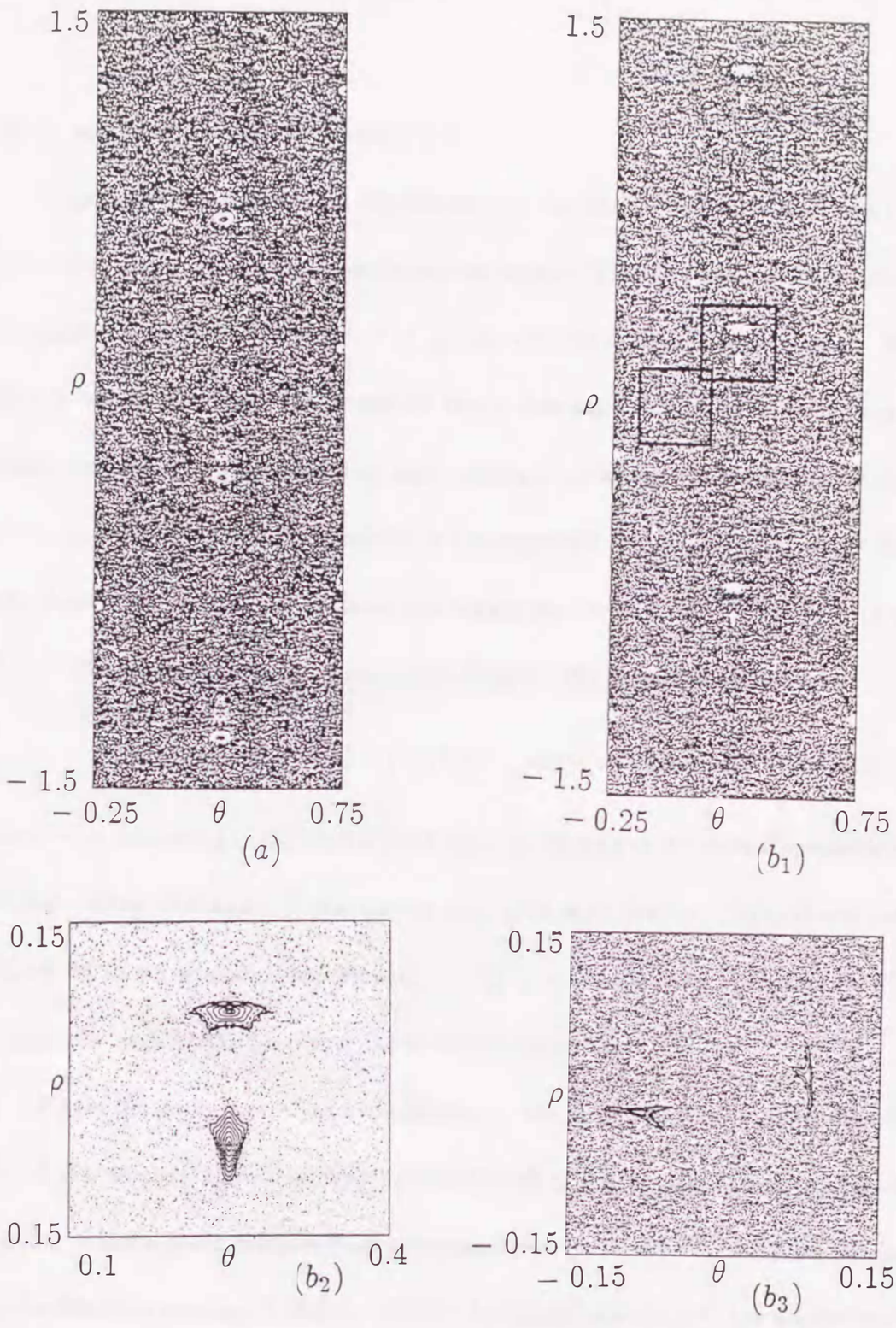

Fig.26 Phase space $\{\theta, \rho\}$ for (a) $A = 0.50$, $d = 0.47$ (the same parameter values as Fig.25), and (b_1) $A = 0.574$, $d = 0.47$. (b_2) The magnification of the normal islands with $v_s = 0$. (b_3) The magnification of the accelerator mode islands with $v_s = 1/2$.

§6.1. Anomalous diffusion with $\zeta > 1$

Figure 27 shows numerical experiments on the variance of $\rho_n - \rho_0 = nv_n(X_0)$ for $A = 0.50$, where no accelerator-mode islands coexist. Thus the linear n-dependence (5.1) is satisfied with a definite value of D unless accelerator-mode islands coexist. We have $D \simeq 0.086$ for $A = 0.50$. The reason for this is that any orbit segment which sticks to an island and encircles the island does not contribute to the sum (5.4) since $[v_n(X_0)]_{\text{torus}} = 0 =< u_t >$. Then (5.4) is determined by the segments of a chaotic orbit which lie inside the chaotic sea, and C_t has a finite correlation time so that (5.5) reduces to (5.1) with $\zeta = 1$. Then the coarse-grained velocity (5.2) obeys the normal distribution

$$P(v;n) = (n/4\pi D)^{1/2} \exp[-nv^2/4D] \tag{6.1}$$

for $n \to \infty$, according to the central limit theorem, leading to the normal spectrum $\psi(v) = v^2/4D$. Then $P(v;n)\,dv = \hat{p}(x)\,dx$ for $x = \sqrt{n}v$ with $\hat{p}(x) = \sqrt{1/4\pi D}\exp[-x^2/4D]$. Figure 28 shows numerical experiments on $\psi_n(v)$ and the scaling of $P(v;n)$ for different values of n with $n \gg 1$, justifying the normal distribution (6.1).

Figure 29 shows numerical experiments on the variance of $\rho_n - \rho_0 = nv_n(X_0)$ for $A = 0.574$, where the accelerator-mode islands with $Q = 3, v_s = 1/2$ coexist. This leads to $\zeta \simeq 1.2$, which is quite different from the normal case $\zeta = 1$. The variance can be analyzed in the following manner. A chaotic orbit in the chaotic sea sticks to the accelerator-mode islands repeatedly with an inverse-power distribution function $f(\tau)$ of sticking times τ; $f(\tau) \propto \tau^{-1-\beta}$, $(2 > \beta > 1)$ for $\tau \gg 1$, where exists a finite mean sticking time $\bar{\tau}$.[5] The

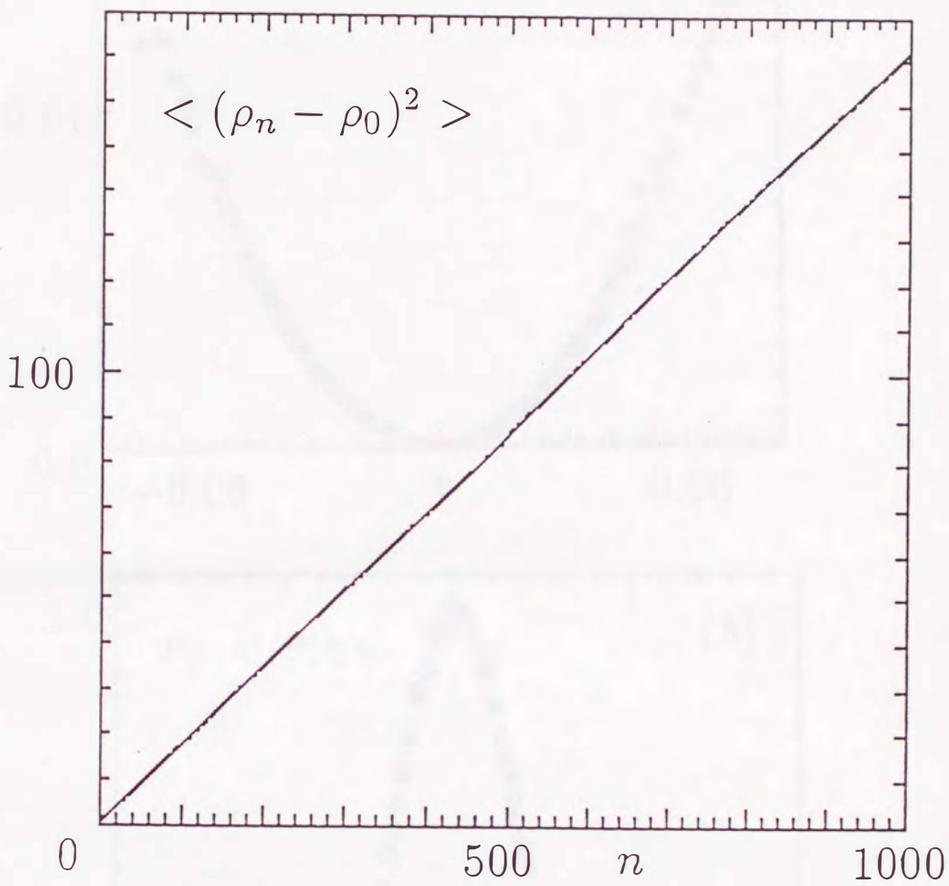

Fig.27 $< (\rho_n - \rho_0)^2 >$ vs n for $A = 0.50$ with $N = 10^5$, where (5.1) is satisfied with $D \simeq 0.086$. $X_0's$ lie on the line $\{-0.25 \leq \theta_0 < 0.75, \rho_0 = 0.0\}$ uniformly.

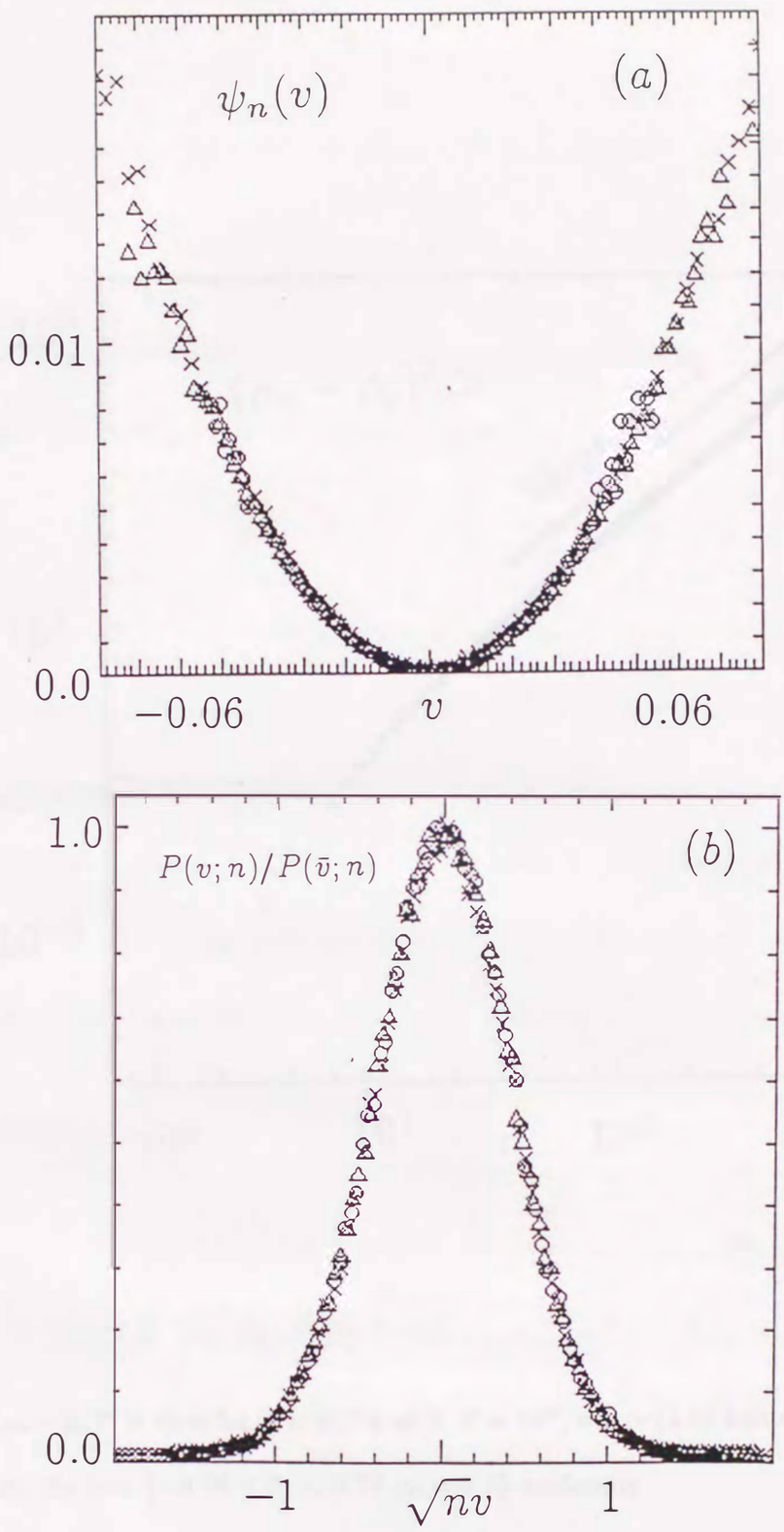

Fig.28 (a) $\psi_n(v)$ vs v and (b) $P(v;n)$ vs $\sqrt{n}\,v$ for $A = 0.50$ with three plots for $n = 250(\times), 500(\triangle)$, $1000(\circ)$ and $N = 10^5$, corresponding to Fig.27. This justifies the normal distribution (6.1).

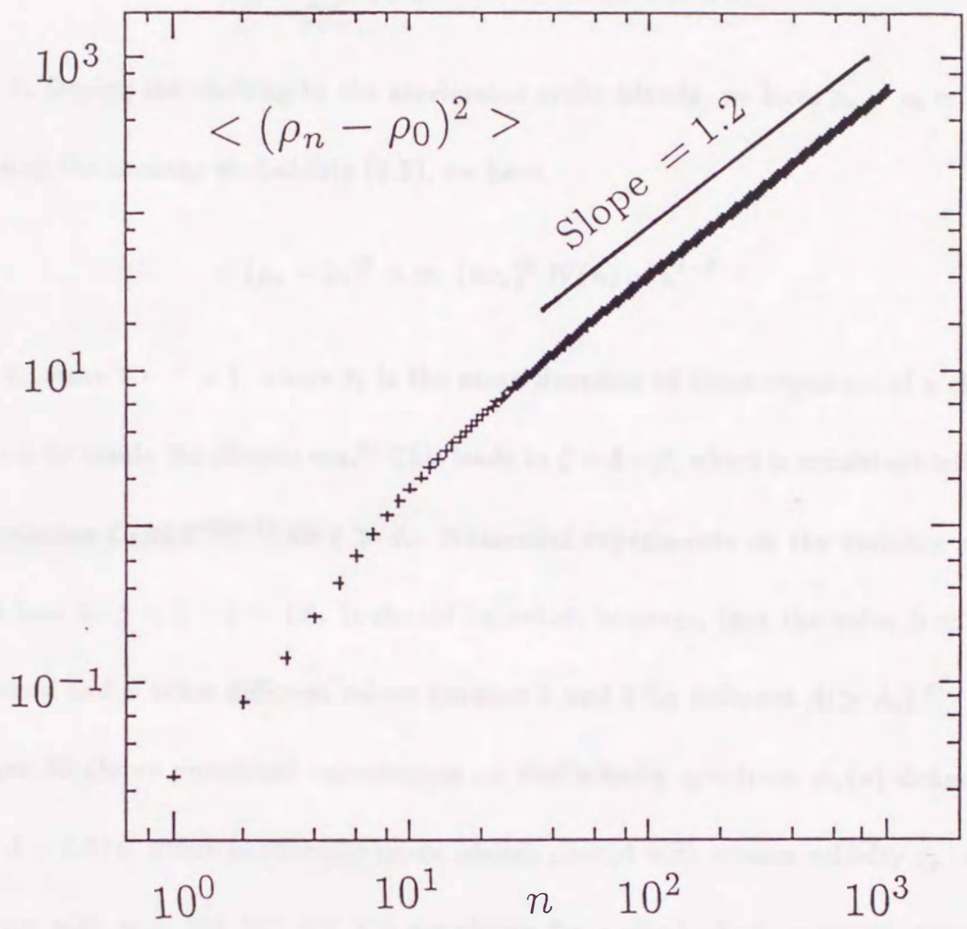

Fig.29 $< (\rho_n - \rho_0)^2 >$ vs n for $A = 0.574$ with $N = 10^5$, where (5.5) holds with $\zeta \simeq 1.2$. $X_0's$ lie on the line $\{-0.25 \leq \theta_0 < 0.75, \rho_0 = 0.1\}$ uniformly.

probability for the chaotic orbit to stick longer than n is given by[4),8)~10)]

$$W(n) \equiv \sum_{\tau=n}^{\infty} \tau f(\tau) \propto n^{-(\beta-1)}, \quad (1 < \beta < 2) \tag{6.2}$$

for $n \gg 1$. During the sticking to the accelerator-mode islands, we have $\rho_n - \rho_0 \simeq \pm n v_s$. Then, using the sticking probability (6.2), we have

$$< (\rho_n - \rho_0)^2 > \simeq (n v_s)^2 \, W(n) \propto n^{3-\beta} \tag{6.3}$$

for $n \gg \bar{\tau}_c$, since $3 - \beta > 1$, where $\bar{\tau}_c$ is the mean duration of those segments of a chaotic orbit which lie inside the chaotic sea.[8)] This leads to $\zeta = 3 - \beta$, which is consistent with the time correlation $C_t \propto t^{-(\beta-1)}$ for $t \gg \bar{\tau}_c$. Numerical experiments on the variance shown in Fig.29 lead to $\beta \simeq 3 - \zeta \simeq 1.8$. It should be noted, however, that the value $\beta \simeq 1.8$ is not universal and β takes different values between 1 and 2 for different $A(> A_c)$.[8)]

Figure 30 shows numerical experiments on the velocity spectrum $\psi_n(v)$ defined by (5.3) for $A = 0.574$, where accelerator-mode islands coexist with stream velocity $v_s = 1/2$. Four curves with $n = 100, 200, 400, 800$ are shown for a cloud of phase points described above (5.1), where $n << N$ must be satisfied. As n increases, the curve of $\psi_n(v)$ becomes flat and approaches the square-well spectrum

$$\psi(v) = \begin{cases} 0 & \text{for} \quad -v_s < v < v_s, \\ \infty & \text{for} \quad |v| > v_s. \end{cases} \tag{6.4}$$

This asymptotic spectrum can be obtained theoretically by using the thermodynamic formalism of $\psi(v)$,[9)] and represents the intermittent switching between the two long streams

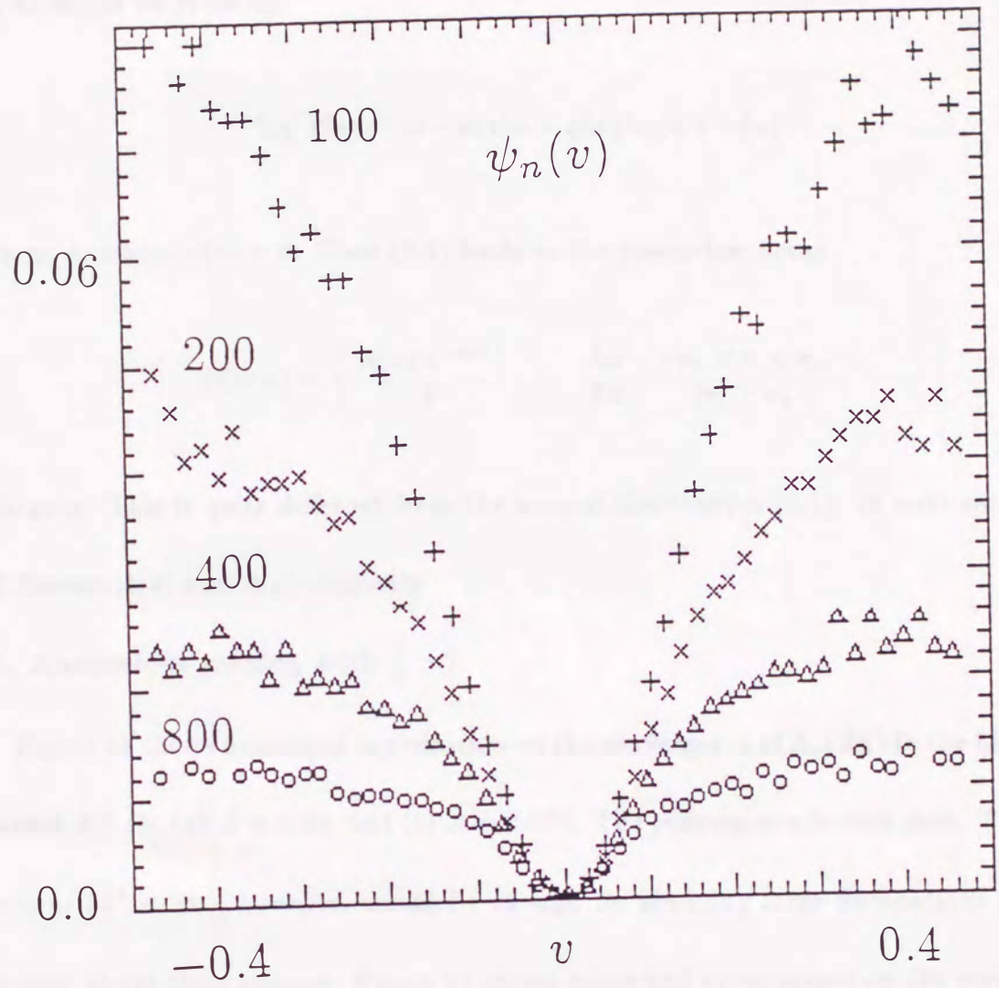

Fig.30 $\psi_n(v)$ vs v for $A = 0.574$, where four plots for $n = 100(+), 200(\times), 400(\triangle), 800(\circ)$ are shown with $N = 10^5$. Plots for $|v| > v_s = 1/2$ are not visible, since their probabilities are extremely small so that their values of $\psi_n(v)$ are extremely high.

$u_t = \pm v_s$ via the chaotic sea.[4] According to the law of large numbers, the general form of $P(v;n)$ would be given by

$$\log P(v;n) = -\psi(v)n - \phi(v)\log n + \alpha(v) \tag{6.5}$$

for large n, where $\phi(v) > 0$. Then (6.4) leads to the power-law decay

$$P(v;n) = \begin{cases} A(v)\, n^{-\phi(v)} & \text{for} \quad -v_s < v < v_s, \\ 0 & \text{for} \quad |v| > v_s \end{cases} \tag{6.6}$$

for large n. This is quite different from the normal distribution (6.1). In next section we shall discuss $A(v)$ and $\phi(v)$ explicitly.

§6.2. Anomalous mixing with $\acute{\zeta} > 1$

Figure 31 shows numerical experiments on the convergence of $\Lambda_n(X_0)$ to the Liapunov exponent Λ^∞ for (a) $A = 0.50$, and (b) $A = 0.574$. The convergence is very slow. The time scale $n = 10^2 \sim 10^3$, however, would be enough for studying large fluctuations of local quantities about their average. Figure 32 shows numerical experiments on the variance of $S_n(X_0)$ for (a) $A = 0.50$ and (b) $A = 0.574$. These justify (5.12) with $\acute{\zeta} \simeq 1.33$ for (a) and $\acute{\zeta} \simeq 1.29$ for (b), which are quite different from the normal case $\acute{\zeta} = 1$.

The variance can be analyzed similarly to the previous. A chaotic orbit in the chaotic sea sticks to the visible islands repeatedly with an inverse-power distribution function $f(\tau)$ of sticking times τ; $f(\tau) \propto \tau^{-1-\acute{\beta}}$, $(2 > \acute{\beta} > 1)$ for $\tau \gg 1$, where exists a finite mean sticking time $\bar{\tau}$.[5] During the sticking to the islands, we have $n\Lambda_n - n\Lambda^\infty \simeq -n\Lambda^\infty$ since

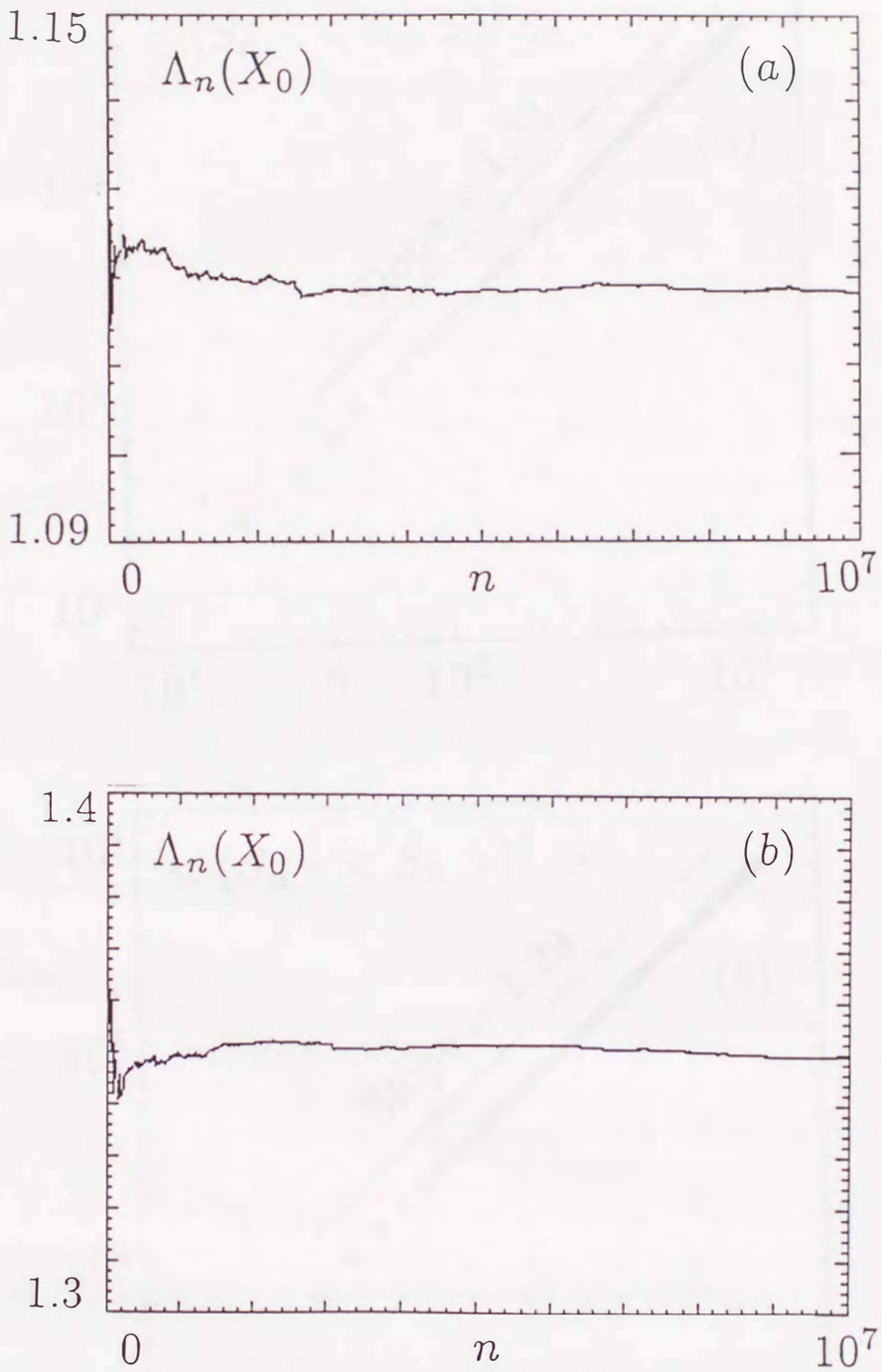

Fig.31 $\Lambda_n(X_0)$ vs $n(=1\sim10^7)$ for (a) $A=0.50$ and (b) $A=0.574$, where $(a)\Lambda^\infty\simeq1.12$ and $(b)\Lambda^\infty\simeq1.35$.

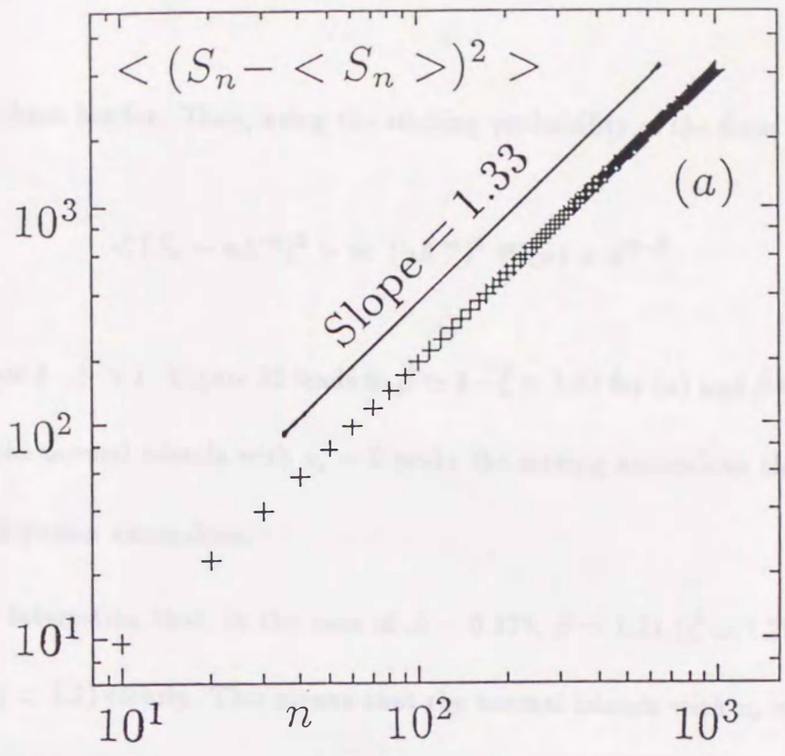

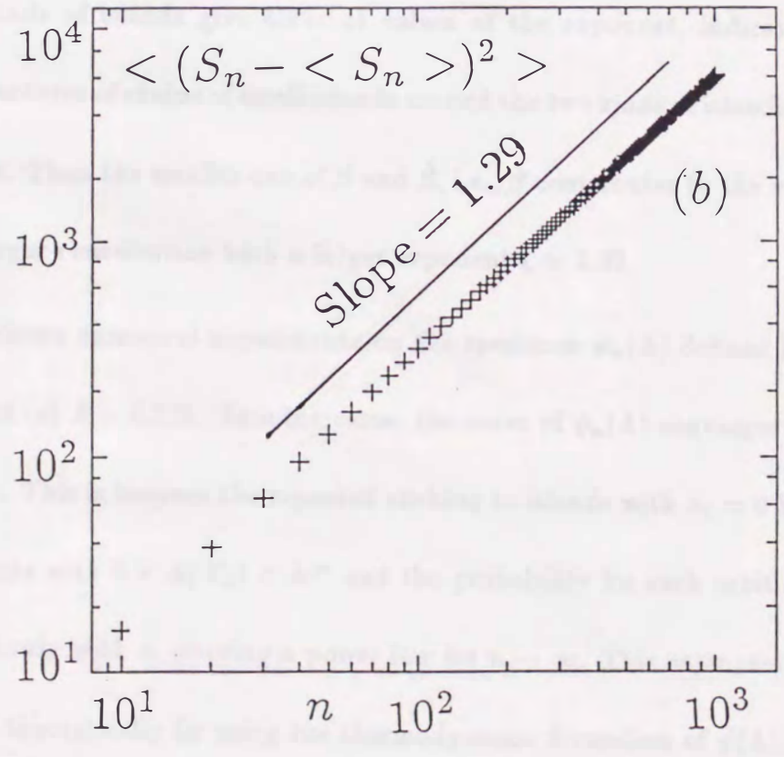

Fig.32 $< (S_n - < S_n >)^2 >$ vs n for (a) $A = 0.50$ and (b) $A = 0.574$ with $N = 10^7$ in (5.9), where (5.11) holds with $(a)\acute{\zeta} \simeq 1.33$ and $(b)\acute{\zeta} \simeq 1.29$.

$\lambda_1 \simeq 0$ in the chaos border. Then, using the sticking probability of the form (6.2), we have

$$< (S_n - n\Lambda^\infty)^2 > \simeq (n\Lambda^\infty)^2 \, W(n) \propto n^{3-\acute{\beta}} \tag{6.7}$$

for $n \gg \bar{\tau}_c$, since $3-\acute{\beta} > 1$. Figure 32 leads to $\acute{\beta} \simeq 3-\acute{\zeta} \simeq 1.67$ for (a) and $\acute{\beta} \simeq 3-\acute{\zeta} \simeq 1.71$ for (b). Thus the normal islands with $v_s = 0$ make the mixing anomalous though they do not make the diffusion anomalous.

It is quite interesting that, in the case of $A = 0.574$, $\acute{\beta} \simeq 1.71$ ($\acute{\zeta} \simeq 1.29$) is different from $\beta \simeq 1.8$ ($\zeta \simeq 1.2$) clearly. This means that the normal islands with $v_s = 0$ produce a larger contribution to the variance (6.7) than the accelerator-mode islands with $v_s = 1/2$, and the two kinds of islands give different values of the exponent, indicating that the hierarchical structures of chains of small islands around the two kinds of islands are different from each other. Then the smaller one of β and $\acute{\beta}$, i.e., $\acute{\beta}$ contributes to the variance (6.7) to produce a larger contribution with a larger exponent $\acute{\zeta} \simeq 1.29$.

Figure 33 shows numerical experiments on the spectrum $\psi_n(\Lambda)$ defined by (5.10) for (a) $A = 0.50$ and (b) $A = 0.574$. As n increases, the curve of $\psi_n(\Lambda)$ converges to $\psi(\Lambda) = 0$ for $0 < \Lambda < \Lambda^\infty$. This is because the repeated sticking to islands with $\lambda_1 = 0$ brings about the orbit segments with $0 < \Lambda(X_0) < \Lambda^\infty$ and the probability for such orbit segments to appear decays slowly with n, obeying a power law for $n \to \infty$. This asymptotic spectrum can be obtained theoretically by using the thermodynamic formalism of $\psi(\Lambda)$.[8)]

According to the law of large numbers, the general form of $P(\Lambda; n)$ for $0 < \Lambda < \Lambda^\infty$

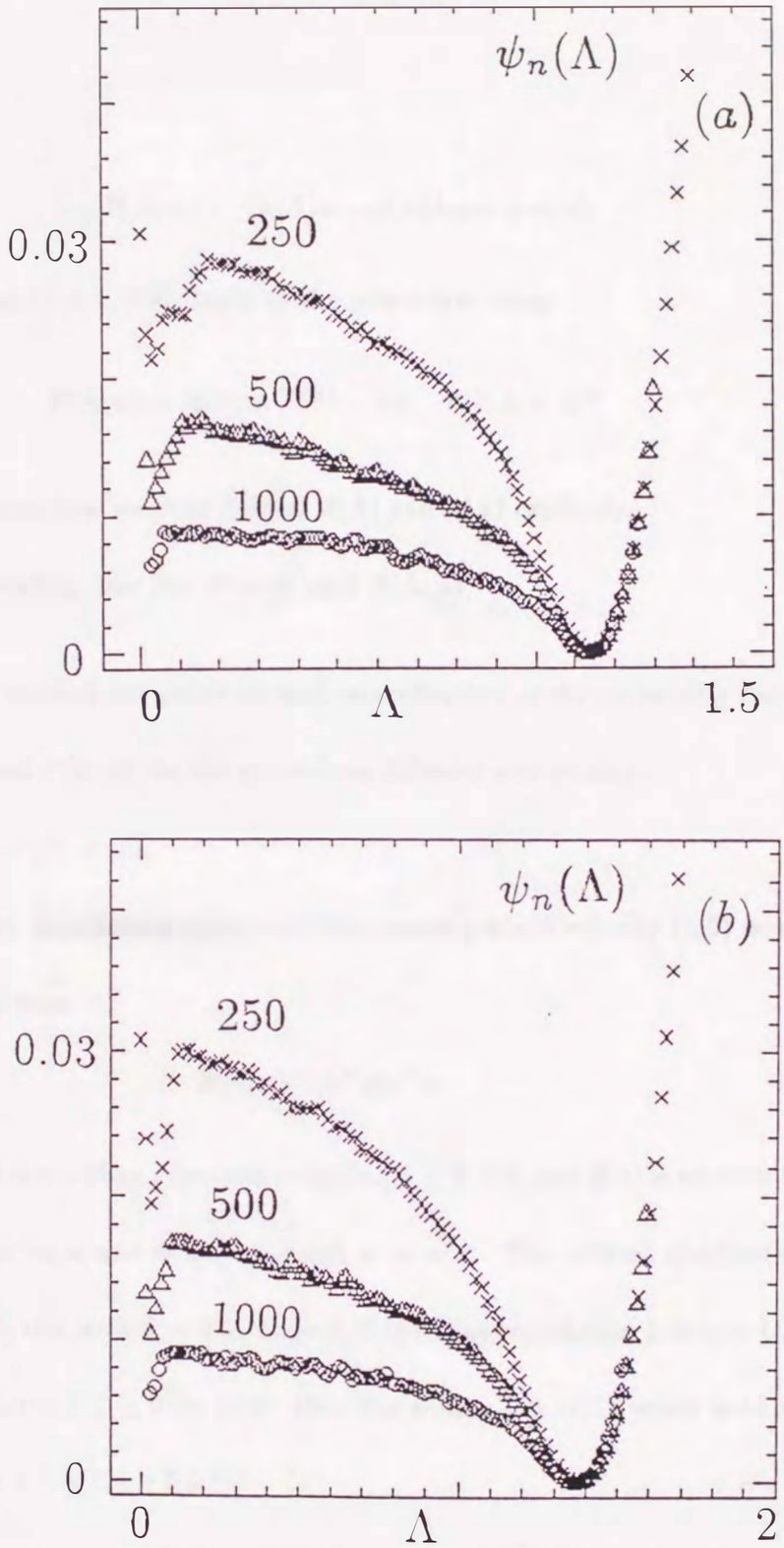

Fig.33 $\psi_n(\Lambda)$ vs Λ for (a) $A = 0.50$ and $(b) A = 0.574$ which show three plots for (a) $n =$ 250($\times$), 500($\triangle$), 1000($\circ$) and (b) $n = 250(\times)$, 500($\triangle$), 1000($\circ$) with $N = 10^7$ in (3.9).

would be given by

$$\log P(\Lambda;n) = -\psi(\Lambda)n - \phi(\Lambda)\log n + \alpha(\Lambda) \tag{6.8}$$

for large n, where $\phi(\Lambda) > 0$. This leads to the power-law decay

$$P(\Lambda;n) = A(\Lambda)\, n^{-\phi(\Lambda)} \quad \text{for} \quad 0 < \Lambda < \Lambda^{\infty} \tag{6.9}$$

for large n. In next section we shall discuss $A(\Lambda)$ and $\phi(\Lambda)$ explicitly.

§7. Anomalous scaling law for $P(v;n)$ and $P(\Lambda;n)$

In this section we shall discuss an anomalous scaling law of the probability distribution functions $P(v;n)$ and $P(\Lambda;n)$ for the anomalous diffusion and mixing.

§7.1. $P(v;n)$ for $-v_s < v < v_s$

The probability distribution function of the coarse-grained velocity (5.2) would obey a scaling law of the form

$$P(v;n) = n^{\delta}\, \hat{p}(n^{\delta}v) \tag{7.1}$$

for large n, where δ is a scaling exponent satisfying $1 \geq \delta > 0$, and $\hat{p}(x)$ is an even function of x which depends on v and n only through $x = n^{\delta}v$. The normal distribution (6.1) satisfies this scaling law with $\delta = 0.5$. Indeed if the time-correlation function C_t decays exponentially so that $1 \geq \zeta \geq 0$ for (5.5), then the scaling law (7.1) would hold with the scaling relation $\delta = 1 - (\zeta/2) \geq 0.5$.[4)]

If C_t has a long-time correlation of the form $C_t \propto t^{-(\beta-1)}, 2 > \beta > 1$ so that $\zeta = 3-\beta > 1$, then the scaling relation $\delta = 1-(\zeta/2) = (\beta-1)/2$ breaks down. Feller's theorem

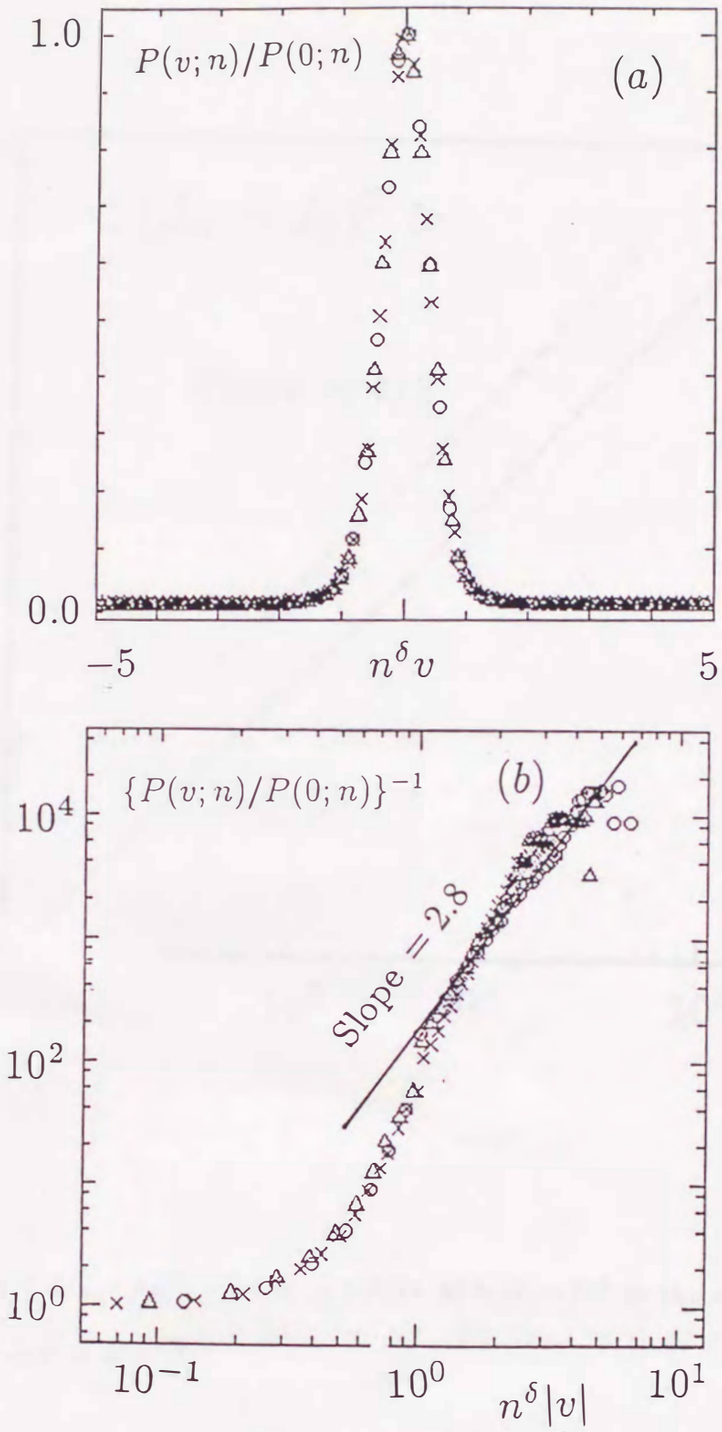

Fig.34 (a) $P(v;n)$ vs $x = n^\delta v$ and (b) $\mathrm{Log}\{P(v;n)/P(\bar{v};n)\}^{-1}$ vs $\mathrm{Log}|x|$ for $A = 0.574$ with three plots for $n = 400(\times)$, $800(\triangle)$, $1600(\circ)$ and $N = 10^5$, where $\delta \simeq 0.44$, $\beta \simeq 1.8$. This justifies the scaling law (7.1) and the asymptotic form (7.3) with exponent $1 + \beta \simeq 2.8$.

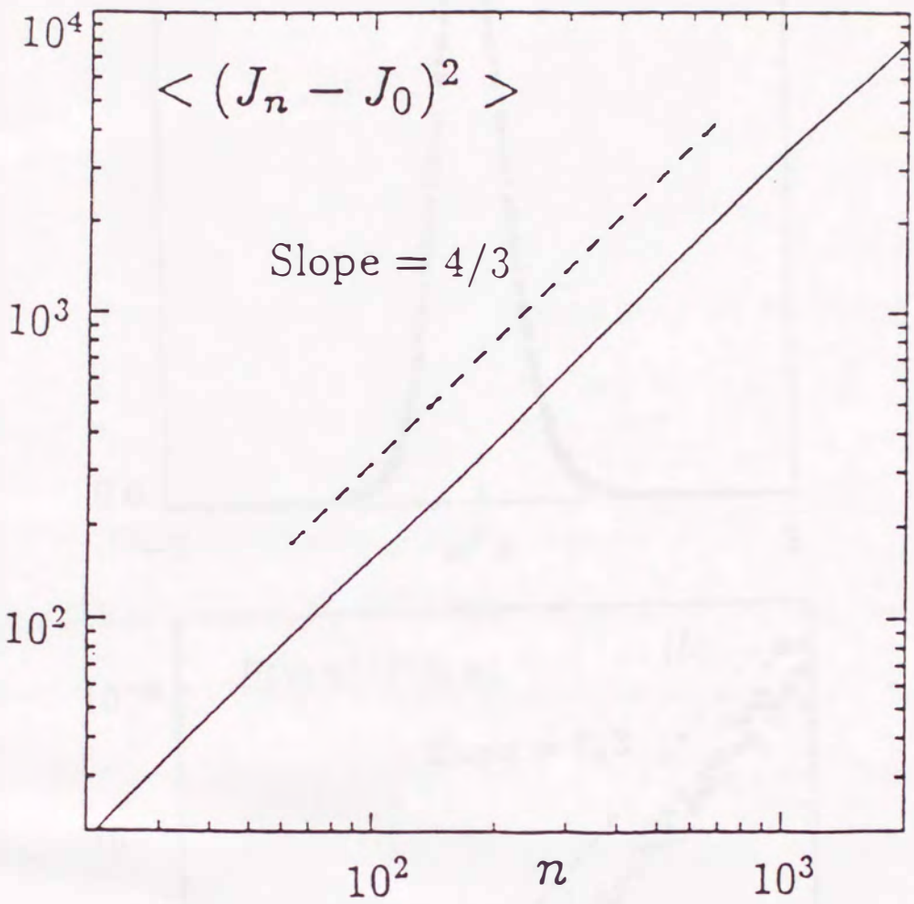

Fig.35 Variance $< (J_n - J_0)^2 >$ for $K = 6.9115$ with $N = 10^5$ in the standard map, where $< (J_n - J_0)^2 > \propto n^{4/3}$.

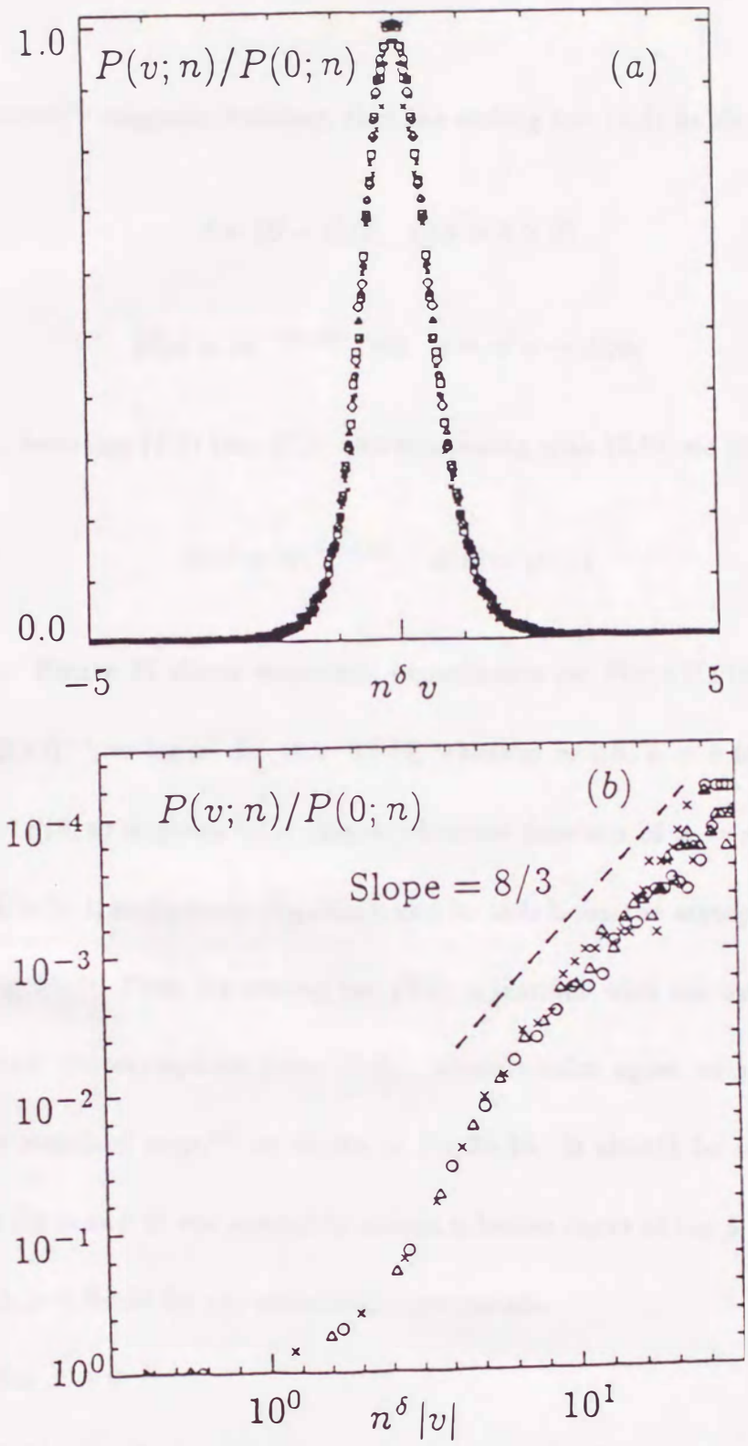

Fig.36 (a) $P(v;n)$ vs $x = n^\delta v$ with five plots for $n = 50(\times)$, $100(\square)$, $200(\diamond)$, $400(\triangle)$, $800(\circ)$ and (b) $\mathrm{Log}[P(v;n)/P(0;n)]$ vs $\mathrm{Log}|x|$ with three plots for $n = 400(\times)$, $800(\triangle)$, $1600(\circ)$ for $K = 6.9115$ with $N = 10^5$ in the standard map, where $\delta = 2/5$, $\beta = 5/3$. This justifies the scaling law (7.1) and the asymptotic form (7.3) with exponent $1 + \beta = 8/3$.

of recurrent events[18] suggests, however, that the scaling law (7.1) holds with

$$\delta = (\beta - 1)/\beta, \quad (0.5 > \delta > 0) \tag{7.2}$$

$$\hat{p}(\boldsymbol{x}) \propto |\boldsymbol{x}|^{-(1+\beta)} \quad \text{for} \quad \boldsymbol{x} = n^{\delta} v \to \pm\infty, \tag{7.3}$$

where $|v| < v_s$. Inserting (7.3) into (7.1) and comparing with (6.6), we obtain

$$A(v) \propto |v|^{-(1+\beta)}, \quad \phi(v) = \beta - 1 \tag{7.4}$$

for $n^{\delta}|v| \to \infty$. Figure 34 shows numerical experiments on $P(v;n)/P(\bar{v};n)$ vs $\boldsymbol{x} = n^{\delta} v$ and $\log\{\hat{p}(\boldsymbol{x})/\hat{p}(\bar{\boldsymbol{x}})\}^{-1}$ vs $\log|\boldsymbol{x}|$ for $A = 0.574$, where $\beta \simeq 1.8$, $\delta \simeq 0.44$. The function $\hat{p}(\boldsymbol{x}) \propto P(v;n)/P(\bar{v};n)$ is given by a unique identical function of $\boldsymbol{x} = n^{\delta} v$ for different values of n with $n \gg 1$, as shown in Fig.34(a), and its tails lie on the asymptotic form (7.3), as seen from Fig.34(b). Thus the scaling law (7.1) is justified with the anomalous scaling relation (7.2) and the asymptotic form (7.3). These results agree with the anomalous diffusion in the standard map,[10] as shown in Fig.35,36. It should be noted that much larger numbers for n and N are needed to obtain a better curve of $\log \hat{p}(\boldsymbol{x})$ vs $\log|\boldsymbol{x}|$ for $\boldsymbol{x} \to \pm\infty$, which is difficult for our numerical experiments.

§7.2. $P(\Lambda;n)$ **for** $\Lambda > 0$

The probability distribution function of the coarse-grained expansion rate (5.8) would also obey a scaling law of the form

$$P(\Lambda;n) = n^{\delta'} p(n^{\delta'}(\Lambda - \Lambda^{\infty})) \quad \text{for} \quad \Lambda > 0. \tag{7.5}$$

If C_t^λ has a long-time correlation of the form $C_t^\lambda \propto t^{-(\acute{\beta}-1)}, 2 > \beta > 1$ so that $\acute{\zeta} = 3 - \acute{\beta} > 1$, then we have the scaling relation

$$\acute{\delta} = (\acute{\beta} - 1)/\acute{\beta}. \quad (0.5 > \acute{\delta} > 0) \tag{7.6}$$

For $0 < \Lambda < \Lambda^\infty$, Feller's theorem indicates that

$$p(x) \propto |x|^{-(1+\acute{\beta})} \quad \text{for} \quad x = n^{\acute{\delta}}(\Lambda - \Lambda^\infty) \to -\infty. \tag{7.7}$$

Inserting (7.7) into (7.5) and comparing with (6.9), we obtain

$$A(\Lambda) \propto |\Lambda - \Lambda^\infty|^{-(1+\acute{\beta})}, \quad \phi(\Lambda) = \acute{\beta} - 1 \tag{7.8}$$

for $n^{\acute{\delta}}(\Lambda - \Lambda^\infty) \to -\infty$.

Figure 37 shows numerical experiments on $\log \{P(\Lambda; n)/P(\Lambda^\infty; n)\}^{-1}$ vs $\log |n^{\acute{\delta}}(\Lambda - \Lambda^\infty)|$ for (a) $A = 0.50$ with $\acute{\delta} \simeq 0.40$, $1 + \acute{\beta} \simeq 2.67$, and (b) $A = 0.574$ with $\acute{\delta} \simeq 0.42$, $1 + \acute{\beta} \simeq 2.71$. Thus the scaling law (7.5) is also justified with the anomalous scaling relation (7.6) and the asymptotic form (7.7).

For $\Lambda > \Lambda^\infty$, we have $p(x) \propto \exp[-ax^{1/\acute{\delta}}]$, $(a > 0)$ for $x >> 1$.[18] This leads to

$$\psi(\Lambda) \propto (\Lambda - \Lambda^\infty)^{1/\acute{\delta}}, \tag{7.9}$$

$$< \Theta(S_n - n\Lambda^\infty)(S_n - n\Lambda^\infty)^2 > \propto n^{\zeta_+}, \quad (\zeta_+ = 2/\acute{\beta}) \tag{7.10}$$

where $\Theta(x)$ is the step function taking 1 for $x > 0$ and 0 for $x < 0$, and $\zeta_+ = 2(1 - \acute{\delta}) = 2/\acute{\beta}$.[19] Since $2/\acute{\beta} < \acute{\zeta} = 3 - \acute{\beta}$, the conditional variance (7.10) is masked in the variance

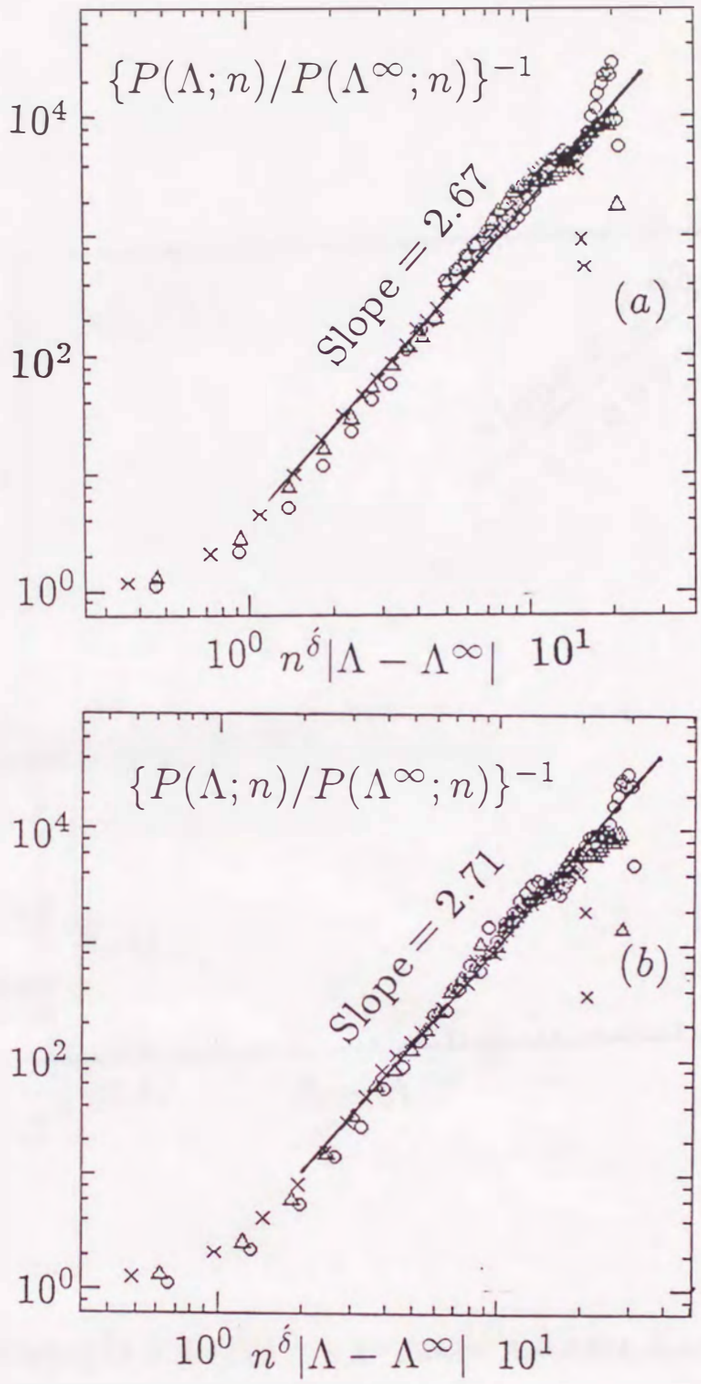

Fig.37 $\mathrm{Log}\{P(\Lambda;n)/P(\Lambda^\infty;n)\}^{-1}$ vs $\mathrm{Log}|n^{\acute{\delta}}(\Lambda - \Lambda^\infty)|$ for $(a)A = 0.50$ and $(b)A = 0.574$ with $(a)\acute{\delta} \simeq 0.40, \acute{\beta} \simeq 1.67$, and $(b)\acute{\delta} \simeq 0.42, \acute{\beta} \simeq 1.71$, which show three plots for (a) $n = 750(\times), 1500(\triangle), 3000(\circ)$ and (b) $n = 750(\times), 1500(\triangle), 3000(\circ)$ with $N = 10^7$ in (5.9). This justifies the scaling law (7.5) and the asymptotic form (7.7) with exponent $(a)1 + \acute{\beta} \simeq 2.67$ and $(b)1 + \acute{\beta} \simeq 2.71$.

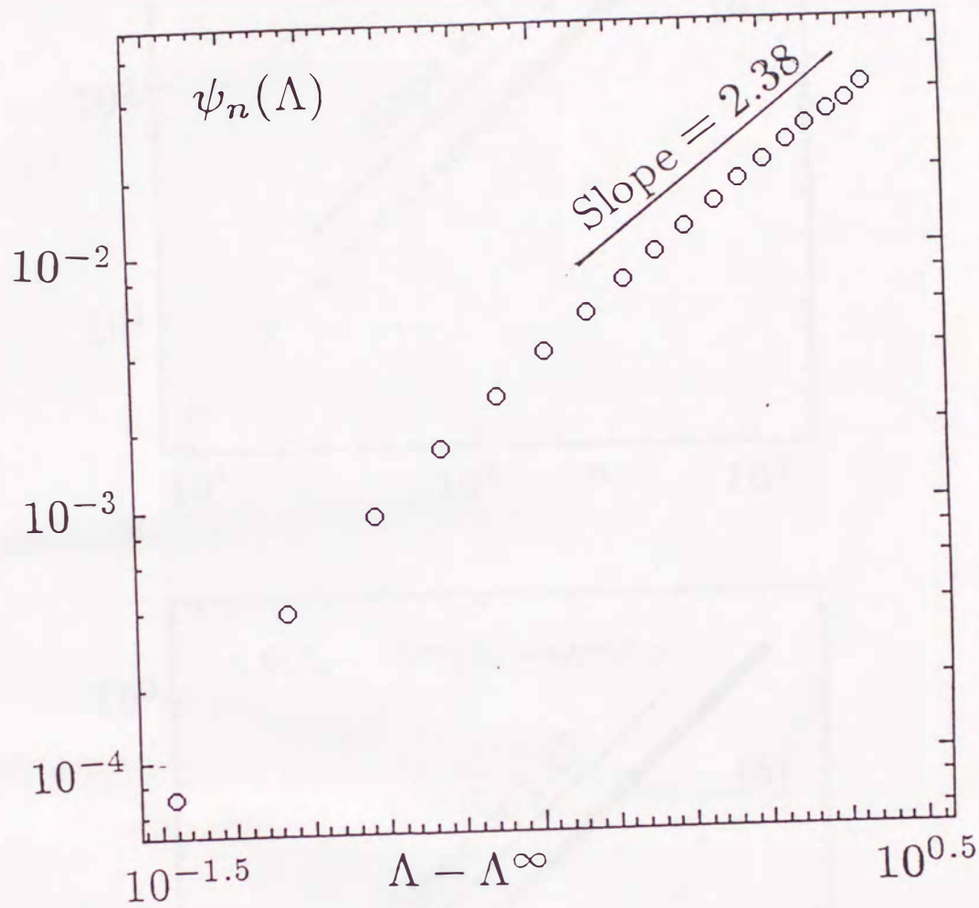

Fig.38 Log $\psi_n(\Lambda)$ vs Log $(\Lambda - \Lambda^\infty)$ for $\Lambda > \Lambda^\infty$, where $A = 0.574$, $n = 250, N = 10^7$. This justifies (7.9) with $1/\acute{\delta} = 2.38$.

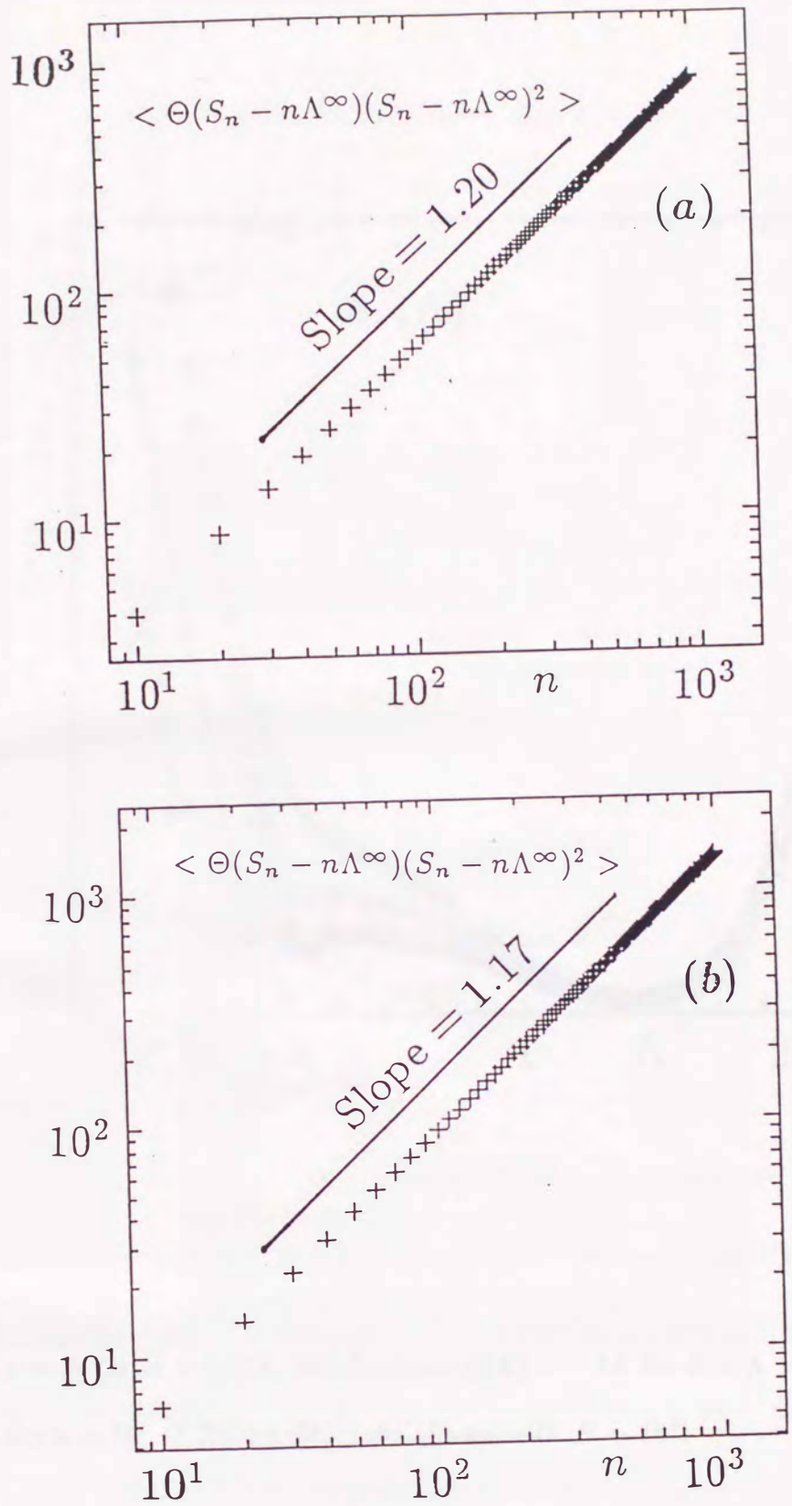

Fig.39 $< \Theta(S_n - n\Lambda^\infty)(S_n - n\Lambda^\infty)^2 >$ vs n for (a) $A = 0.50$ and (b) $A = 0.574$ with $N = 10^7$, where (7.10) holds with (a) $\zeta_+ \simeq 1.20$ and (b) $\zeta_+ \simeq 1.17$.

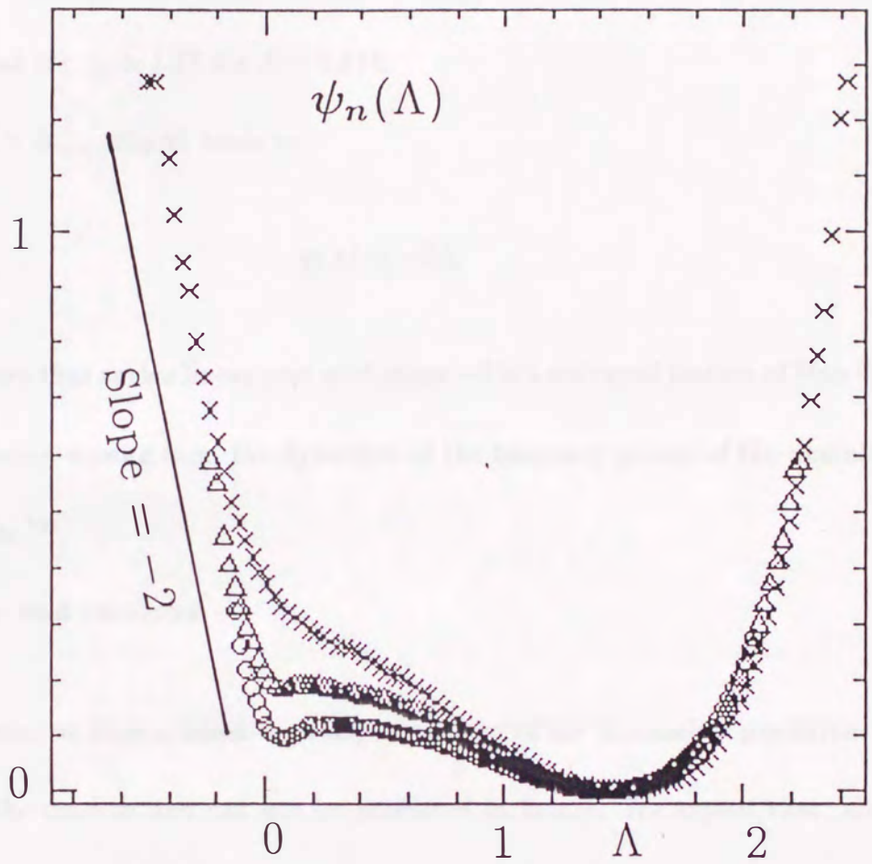

Fig.40 $\psi_n(\Lambda)$ vs Λ for $A = 0.574$, which shows $\psi(\Lambda) = -2\Lambda$ for $0 > \Lambda > \Lambda_{\min}$. Here three plots for $n = 10(\times), 20(\triangle), 40(\circ)$ are shown with $N = 10^7$.

(6.7) by the fluctuations in the region $\Lambda^{\infty} > \Lambda > 0$. Figure 38 justifies (7.9) numerically for $A = 0.574$ with $1/\acute{\delta} \simeq 2.38$. Figure 39 justifies (7.10) numerically, where (a) $\zeta_{+} \simeq 1.20$ for $A = 0.50$ and (b) $\zeta_{+} \simeq 1.17$ for $A = 0.574$.

For $0 > \Lambda > \Lambda_{\min}$, Fig.40 leads to

$$\psi(\Lambda) = -2\Lambda. \tag{7.11}$$

It has been shown that such a linear part with slope -2 is a universal feature of Hamiltonian dynamical systems, arising from the dynamics of the tangency points of the unstable and stable manifolds.[19)]

§8. Summary and remarks

In this thesis, we have studied the complex motion of the frictionless pendulum whose motion looks like random and can not be predicted in future. We expect that, although each of the chaotic orbits is unstable and unreproducible, their ensemble and long-time average over each orbit are stable and reproducible. We have concretely studied the anomalous behaviors of the diffusion and mixing of chaotic orbits due to the intermittent sticking to the islands of tori in terms of the fluctuations of the coarse-grained velocity $v_n(X_0)$ and the coarse-grained expansion rate $\Lambda_n(X_0)$ by taking the standard map and the heating map which exhibit their remarkable features clearly. It is well-known that the distribution function is Gaussian if the motion is completely random. It is interesting that the distribution function is very different from the Gaussian.

Table I is shows the comparison between the diffusion and mixing of chaotic orbits according to parameter A.

	Diffusion		Mixing	
$A(A > A_c)$	Variance of S_n	Distribution Function of $P(v;n)$	Variance of S_n	Distribution Function of $P(\Lambda;n)$
Normal Islands	$\propto n$	Gaussian	$\propto n^{3-\acute{\beta}}$	Non Gaussian
Accelerator-Mode Islands	$\propto n^{3-\beta}$	Non Gaussian	$\propto n^{3-\acute{\beta}}$	Non Gaussian
No Islands	$\propto n$	Gaussian	$\propto n$	Gaussian

Table I.

It is supposed that the distribution function of the sticking time of chaotic orbits around the torus is an inverse-power distribution $f(t) \sim t^{-1-\beta}$.[5] What we wanted to study is the relation between the statistics which are the distribution function of sticking time of chaotic orbits, the variance and the distribution function of the coarse-grained velocity v_n and coarse-grained expansion rate Λ_n. We have found that the probability distribution functions for the fluctuations of $v_n(X_0)$ and $\Lambda_n(X_0)$ obey an identical anomalous scaling law of the form (7.1) and (7.5) with $0.5 > \delta, \acute{\delta} > 0$, and the scaling exponents $\delta, \acute{\delta}$ are given by (7.2) and (7.6), where $\beta, \acute{\beta}$ can be obtained from the variances. The anomaly is brought about by the intermittent sticking of chaotic orbits to the islands of tori. There exist two kinds of islands of tori with streaming velocity $v_s > 0$ (accelerator-mode islands) and $v_s = 0$ (normal islands), depending on the bifurcation parameter A. Both of these islands produce a long-time correlation of chaotic orbits, leading to anomalous statistical

properties.

The two kinds of islands, however, produce different contributions to the diffusion and the mixing. The statistical properties of the diffusion and mixing are different at even the same value of parameter A; indeed, we have $\beta = 2, \delta = 0.5, \acute{\beta} = 1.67, \acute{\delta} = 0.40$ for $A = 0.50, d = 0.47$ where no accelerator-mode islands coexist, and $\beta = 1.8, \delta = 0.44, \acute{\beta} = 1.71, \acute{\delta} = 0.42$ for $A = 0.574, d = 0.47$ where accelerator-mode islands coexist. The reason is the following. For $A = 0.50$, the value ($\simeq 0$) of v_n in the chaos border is equal to the average value $\bar{v}_n (= 0)$, whereas the value ($\simeq 0$) of Λ_n in the chaos border is different from the average value $\Lambda^{\infty} (\simeq 1.09)$. This leads to the fact that the diffusion is normal, whereas the mixing is anomalous. For $A = 0.574$, however, the value ($= \pm v_s$) of v_n in the chaos border with the accelerator-mode islands is different from the average value $\bar{v}_n (= 0)$, so that both the diffusion and the mixing become anomalous. The values of β and $\acute{\beta}$ are, however, different from each other, since the accelerator-mode islands and the coexisting normal islands have different structures of the islands-around-islands hierarchy. Indeed, the numerical experiments imply that the coexisting normal islands produce a larger contribution to the variance of $S_n = n\Lambda_n(X_0)$ than the accelerator-mode islands, and the deviation $\triangle\zeta \equiv \zeta - 1 = 2 - \beta$ is produced by the accelerator-mode islands, whereas $\triangle\acute{\zeta} \equiv \acute{\zeta} - 1 = 2 - \acute{\beta}$ is produced by the normal islands in the both cases of $A = 0.50$ and $A = 0.574$.

Thus the statistical properties of chaotic orbits in a chaotic sea are drastically influ-

enced by what kinds of islands exist in the chaotic sea. The sticking time is an inverse-power law which is slower than the exponential decay. This is due to the hierarchical structure of torus. But the relation between the geometrical structure of torus and the power β is not clear.

These anomalous statistical properties are expected to hold for other two-dimensional maps which are periodic in action. We have shown that such anomalous features hold for both the standard map and the heating map.[8)~10)] It is also worth noting that such anomalous properties of the mixing and diffusion have been found observable even in the time-dependent laminar flows such as oscillating Rayleigh-Bénard convection with a large aspect ratio whose Poincaré map is periodic in the roll position.[11),20)] Thus it turns out that these statistical properties of the mixing and diffusion of chaotic orbits give the universal features which are generally valid for the widespread Lagrangian turbulence of fluids as well as the widespread chaos of the two-dimensional periodic maps. In order to establish this important fact, however, we need further investigation from the viewpoint of dynamical systems.

Acknowledgements

I am very grateful to Professor Hazime Mori. Prof. H. Mori has guided me studies in this thesis and has given me a clear description even since his retirement from Kyushu University. I also wish to thank Prof. H. Fujisaka, Prof. H. Okamoto, Prof. T. Yoshida and all others of our chaos group at Kyushu University for stimulating discussions.

I was very helped by Dr. T. Horita's advanced studies. Dr. H. Shibata gave me many advises to write this thesis.

This study was partially financed by the Grant-in-Aid for Scientific Research of Ministry of Education, Science and Culture.

Appendix A. Derivation of the diffusion equation for two-dimensional maps

In the nonlinear two-dimensional maps, the diffusion of the chaotic orbits occurs in action when the nonlinear parameter exceeds a critical value (for example, standard map for $K > K_c(= 0.97163...)$ and heating map for $A > A_c$ $(= 0.20565...)$). To study the statistical properties of the behavior of chaotic orbits, we consider the distribution function of only action direction. Let $P(J;n)$ be the probability distribution function for $J(X_t)$ and suppose that the distribution function obeys a Markoff process. The evolution of this distribution function is given by the equation

$$P(J, n + \Delta n) = \int P(J - \Delta J, n) W_n(J - \Delta J, \Delta J, \Delta n) d(\Delta J), \qquad (A.1)$$

where $W(J, n, \Delta J, \Delta n)$ is the transition probability which the probability distribution function to take J at n increase by ΔJ after Δn. The expansion of PW_n to second order is

$$P(J - \Delta J) W_n(J - \Delta J) = P(J) W_n(J) - \frac{\partial (PW_n)}{\partial J} (\Delta J)$$

$$+ \frac{1}{2} \frac{\partial^2 (PW_n)}{\partial J^2} (\Delta J)^2. \qquad (A.2)$$

The transition probability satisfies the condition

$$\int W_n(J, n, \Delta J, \Delta n)\ d(\Delta J) = 1. \qquad (A.3)$$

Thus we obtain the Fokker-Plank equation

$$\frac{\partial P}{\partial n} = -\frac{\partial (BP)}{\partial J} + \frac{1}{2} \frac{\partial^2 (DP)}{\partial J^2}, \qquad (A.4)$$

where B is the friction coefficient and D is the diffusion constant. These are

$$B(J) = \frac{1}{\Delta n} \int \Delta J \;\; W_n(J, n, \Delta J, \Delta n) d(\Delta J), \tag{A.5}$$

$$D(J) = \frac{1}{\Delta n} \int (\Delta J)^2 W_n(J, n, \Delta J, \Delta n) d(\Delta J). \tag{A.6}$$

Landau derived the following relation B and D

$$B = \frac{1}{2} \frac{dD}{dJ} \tag{A.7}$$

for Hamiltonian system. The Fokker-Plank equation can be rewritten in the following diffusion equation

$$\frac{\partial P}{\partial n} = \frac{\partial}{\partial J}(\frac{D}{2} \frac{\partial P}{\partial J}). \tag{A.8}$$

The diffusion constant is

$$D = \frac{1}{2} \int (J_n - J_0)^2 W(J, \theta, n | J_0, \theta_0, 0) d(\Delta\theta) d(\Delta J) \tag{A.9}$$

for $n \to \infty$.

Appendix B. Derivation of the local expansion rate $\lambda_1(X_t)$ in the heating map

To determine $\lambda_1(X_t)$ we define a reference trajectory (u_t, v_t). We consider a neighboring trajectory $(u_t + \delta u_t, v_t + \delta v_t)$, where δu_t and δv_t are infinitesimals. Then, δu_t and δv_t satisfy

$$\begin{bmatrix} \delta u_{t+1} \\ \delta v_{t+1} \end{bmatrix} = DF(X_t) \begin{bmatrix} \delta u_t \\ \delta v_t \end{bmatrix}, \tag{B.1}$$

where

$$DF(X_t) = \begin{bmatrix} 1 & 2\pi A \sin 2\pi v_t \\ -2\pi A \sin 2\pi u_{t+1} & 1 - (2\pi A)^2 \sin 2\pi u_{t+1} \sin 2\pi v_t \end{bmatrix}$$

for the heating map. Eigenvalues of matrix $DF(X_t)$ are

$$\lambda_{\pm} = \frac{-\{(2\pi A)^2 \sin(2\pi u_{t+1}) \sin(2\pi v_t) - 2\} \pm \sqrt{\{(2\pi A)^2 \sin(2\pi u_{t+1}) \sin(2\pi v_t) - 2\}^2 - 4}}{2}. \tag{B.2}$$

The vector tangent to the local unstable manifold at X_t is

$$\begin{cases} \delta u_t^* = 2\pi A \sin(2\pi v_t), \\ \\ \delta v_t^* = \lambda_+ - 1. \end{cases} \tag{B.3}$$

The unit vector $u_1(X_t)$ is

$$\frac{1}{\sqrt{\delta u_t^{*2} + \delta v_t^{*2}}} \begin{bmatrix} \delta u_t^* \\ \delta v_t^* \end{bmatrix}. \tag{B.4}$$

Since the local expansion rate $\lambda_1(X_t)$ is the rate of increase of vector to the local unstable manifold at X_t, $\lambda_1(X_t)$ is given by

$$\log l_{t+1}/l_t, \tag{B.5}$$

where

$$l_t = \sqrt{\delta u_t^{*2} + \delta v_t^{*2}}.$$

Then the local expansion rate $\lambda_1(X_t)$ is given by

$$\lambda_1(X_t) \equiv \log |DF(X_t) u_1(X_t)|. \tag{B.6}$$

Appendix C. Derivation of (6.2)[5)]

Suppose that the total length which chaotic orbits stick to islands is T and N_τ is the number of segments of length τ. Then we have $\sum \tau N_\tau = T$. The distribution function $f(\tau)$ of sticking time τ is given by

$$f(\tau) = \frac{N_\tau}{T}. \tag{C.1}$$

Since the distribution function $f(\tau)$ are therefore normalized so that $\sum \tau f(\tau) = 1$, the probability which has segment length τ is

$$P(\tau) = \frac{\tau N_\tau}{T}. \tag{C.2}$$

Then the probability for the chaotic orbit to stick longer than n is given by

$$W(n) = \sum_{\tau=n}^{\infty} \tau f(\tau). \tag{C.3}$$

If we suppose that the distribution function obeys inverse-power law $f(\tau) \propto \tau^{-1-\beta}$, we obtain

$$W(n) \propto n^{-(\beta-1)} \tag{C.4}$$

by integrate (C.3).

References

[1] A. J. Lichtenberg and M.A. Lieberman, *Regular and Stochastic Motion* (Springer-Verlag, New York, 1982).

[2] R.S. MacKay and J.D. Meiss, *Hamiltonian Dynamical Systems* (Adam Hilger, Bristol, 1987).

[3]) Pierre Bergé, Yves Pomeau, Christian Vidal, *Order Within Chaos* (Wiley,New York, 1984).

H. G. Schuster, *Deterministic Chaos* (VCH, Weinheim, 1988).

S. N. Rasband, *Chaotic Dynamics of Nonlinear Systems* (John Wiley, New York, 1990).

[4] H. Mori, H. Hata, T. Horita and T. Kobayashi, Prog. Theor. Phys. Suppl. **99**(1989), 1, and references cited therein.

[5] C. F. F. Karney, Physica **8D**(1983), 360.

B.V. Chirikov and D.L. Shepelyansky, Physica **13D**(1984), 395.

J.D. Meiss and E. Ott, Phys. Rev. Lett. **55**(1985), 2741; Physica **20D**(1986), 387.

[6] H. Aref, J. Fluid Mech. **143**(1984), 1.

J. Chaiken, R. Chevray, M. Tabor and Q. M. Tan, Proc. R. Soc. Lond. **A408**(1986), 165.

[7] T. H. Solomon and J. P. Gollub, Phys. Rev. **A38**(1988), 6280.

D. S. Broomhead and S. C. Ryrie, Nonlinearity **1** (1988), 409.

[8] T. Horita, H. Hata, R. Ishizaki and H. Mori, Prog. Theor. Phys. **83**(1990), 1065.

[9] R. Ishizaki, H. Hata, T. Horita and H. Mori, Prog. Theor. Phys. **84**(1990), 179.

[10] R. Ishizaki, T. Horita, T.Kobayashi and H. Mori, Prog. Theor. Phys. **85**(1991), 1013.

[11] K. Ouchi, N. Mori, T. Horita and H. Mori, Prog. Theor. Phys. **85**(1991), 687.

[12] H. Mori, H. Okamoto and H. Tominaga, Prog. Theor. Phys. **85**(1991), 1143.

[13] C. F. F. Karney: Phys. Fluids **21**(1978), 1584 and **22** (1979), 2188.

[14] J. M. Greene, J. Math. Phys. **20**(1979), 1183.

[15] A. J. Lichtenberg and M. A. Lieberman, Physica **D33**(1988), 211, and references cited therein.

[16] Y. H. Ichikawa, T. Kamimura and T. Hatori, Physica **29D**(1987), 247.

[17] Y. H. Ichikawa, Y. Nomura and T. Kamimura, Prog. Theor. Phys. Suppl. **99**(1989), 220.

[18] W. Feller, Trans. Am. Math. Soc. **67**(1949), 98.

X.-J. Wang, Phys. Rev. **A39**(1989), 3214.

[19] T. Horita and H. Mori, in *From Phase Transitions to Chaos*, edited by G.Györgi et al (World Scientific, Singapore, 1992).

[20] K.Ouchi and H. Mori, Prog. Theor. Phys. **88**(1992), 467.

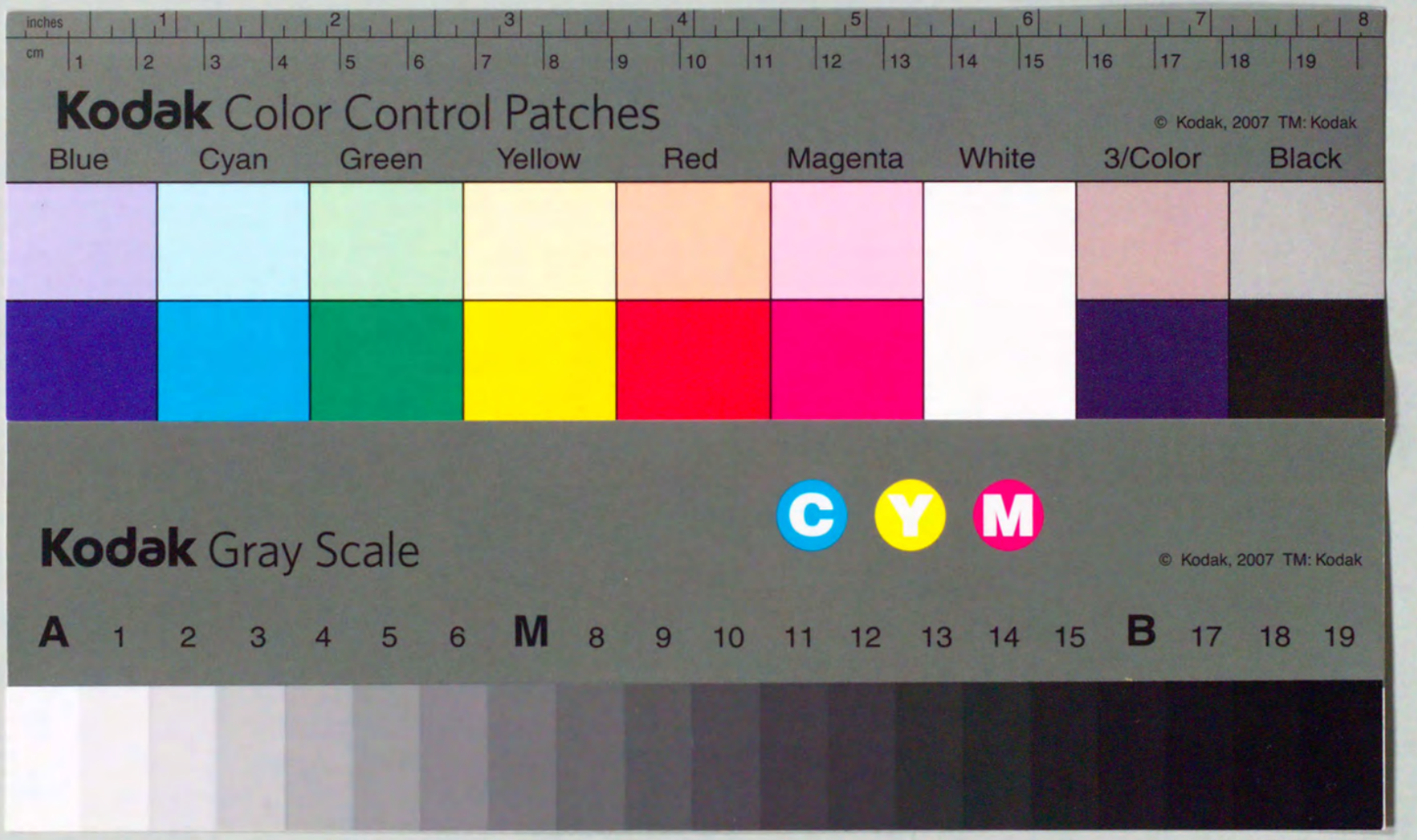
inches
cm
Kodak Color Control Patches
© Kodak, 2007 TM: Kodak
Blue
Cyan
Green
Yellow
Red
Magenta
White
3/Color
Black
Kodak Gray Scale
C
Y
M
© Kodak, 2007 TM: Kodak
A 1 2 3 4 5 6 M 8 9 10 11 12 13 14 15 B 17 18 19